

See discussions, stats, and author profiles for this publication at: <https://www.researchgate.net/publication/284358620>

# Review on the recent improvements in sonochemical and combined sonochemical oxidation processes – A powerful tool for destruction of environmental contaminants

Article in *Renewable and Sustainable Energy Reviews* · March 2016

DOI: 10.1016/j.rser.2015.10.139

CITATIONS

42

READS

1,115

3 authors, including:



**Panneerselvam Sathishkumar**

Aksum University

44 PUBLICATIONS 1,181 CITATIONS

[SEE PROFILE](#)



**Anandan Sambandam**

National Institute of Technology Tiruchirappalli

315 PUBLICATIONS 5,652 CITATIONS

[SEE PROFILE](#)

Some of the authors of this publication are also working on these related projects:



Solar cells [View project](#)



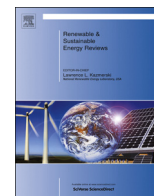
Bacteriorhodopsin for Dye Sensitized solar Cells [View project](#)



ELSEVIER

Contents lists available at ScienceDirect

## Renewable and Sustainable Energy Reviews

journal homepage: [www.elsevier.com/locate/rser](http://www.elsevier.com/locate/rser)

## Review on the recent improvements in sonochemical and combined sonochemical oxidation processes – A powerful tool for destruction of environmental contaminants

Panneerselvam Sathishkumar<sup>a,b,\*</sup>, Ramalinga Viswanathan Mangalaraja<sup>a,\*\*</sup>, Sambandam Anandan<sup>c</sup><sup>a</sup> Advanced Ceramics and Nanotechnology Laboratory, Department of Materials Engineering, Faculty of Engineering, University of Concepcion, Concepcion 407-0409, Chile<sup>b</sup> Department of Chemistry, Periyar Maniammai University, Vallam, Thanjavur 613403, Tamil Nadu, India<sup>c</sup> Nanomaterials and Solar Energy Conversion Lab, Department of Chemistry, National Institute of Technology, Trichy 620015, India

## ARTICLE INFO

## Article history:

Received 31 January 2014

Received in revised form

13 August 2015

Accepted 26 October 2015

## Keywords:

Ultrasound

Sonochemistry

Combined AOPs

Sonoreactor set up

Wastewater treatment

## ABSTRACT

The last two decades research demonstrate that the presence of organic contaminants in drinking water has increased every year and the increasing demand for the technology to reclaim the water from the effluents released by the industries has persuaded us to write the review in this topic. The combination of advanced oxidation processes (AOPs) namely photocatalysis, Fenton and ozonolysis combined with sonolysis harvests the degradation of wide spectrum of organic contaminants. The various parameters including the geometry of the sonochemical reactors influencing the sonochemical reactions have been discussed. The combination of sonolysis with photocatalysis, Fenton and ozonolysis enhances the production of non-selective radicals to improve the degradation process thus avoiding the secondary pollution. The economical and technical feasibilities of the AOPs are very essential for the initialization of the combined AOPs for the degradation of environmental contaminants. The review envisions to improve our understanding and outline directions for future research.

© 2015 Elsevier Ltd. All rights reserved.

## Contents

1. Introduction	426
2. Sonolysis	431
2.1. Factors influencing acoustic cavitation	432
3. Geometry of sonochemical reactors for the enhanced degradation of environmental pollutants	433
4. Combined sonophotocatalytic degradation of environmental pollutants	434
4.1. Photocatalysis	434
4.2. Sonophotocatalysis	436
5. Combined sono, photo, electro, Fenton processes for the degradation of environmental pollutants	441
6. Combined sonolysis with ozonolysis process for the degradation of environmental pollutants	446
7. Conclusions	449
Acknowledgments	450
References	450

\* Corresponding author at: Advanced Ceramics and Nanotechnology Laboratory, Department of Materials Engineering, Faculty of Engineering, University of Concepcion, Concepcion 407-0409, Chile. Tel.: +56 41 2207389; fax: +56 41 2203391.

\*\* Corresponding author. Tel.: +56 41 2207389; fax: +56 41 2203391.

E-mail addresses: [sathish\\_panner2001@yahoo.com](mailto:sathish_panner2001@yahoo.com) (P. Sathishkumar), [mangal@udec.cl](mailto:mangal@udec.cl) (R.V. Mangalaraja).

## 1. Introduction

In the forthcoming years, worldwide crisis may arise for energy, food and water; however, the three are inter-connected and water is essential for all social and economic developments among the nations [1]. During the past two decades, considerable increase in the concentration of organic contaminants in surface water has been observed [2,3]. On the other hand diseases spread through

**Table 1**  
Some reactions involved in advanced oxidation processes [19,20].

Advanced oxidation process	Reaction steps
<b>Sonolysis</b>	$H_2O \rightarrow \cdot OH + OH^-$ $H_2O \rightarrow (1/2)H_2 + (1/2)H_2O_2$
<b>Semiconductor photocatalysis (TiO<sub>2</sub>-semiconductor)</b>	$TiO_2 + h\nu \rightarrow TiO_2^- + \cdot OH$ (or $TiO_2^+$ ) $TiO_2^- + O_2 + H^+ \rightarrow TiO_2 + \cdot OH + H_2O$ $TiO_2^- + 2H^+ \rightarrow TiO_2 + \cdot H_2$ $H^+ + H_2O \rightarrow \cdot OH + H^+$
<b>Fenton reactions</b>	$Fe^{2+} + H_2O_2 \rightarrow Fe^{3+} + \cdot OH + OH^-$
<b>Ozonolysis</b>	$O_3 + H_2O \rightarrow 2HOO\cdot$ $O_3 + 2HOO\cdot \rightarrow \cdot OH + 2O_2$
<b>Sonophotocatalysis (with H<sub>2</sub>O<sub>2</sub>)</b>	
(i) <b>Water sonolysis</b>	$H_2O \rightarrow \cdot OH + OH^-$ $H_2O \rightarrow (1/2)H_2 + (1/2)H_2O_2$
(ii) <b>Reaction of H<sub>2</sub>O<sub>2</sub> with H atoms (formed from water sonolysis)</b>	$H_2O_2 + H\cdot \rightarrow H_2O + \cdot OH$
(iii) <b>Photolytic dissociation of H<sub>2</sub>O<sub>2</sub></b>	$H_2O_2 + h\nu \rightarrow 2\cdot OH$
(iv) <b>Reaction of H<sub>2</sub>O<sub>2</sub> with superoxides (formed in the presence of TiO<sub>2</sub> and under UV irradiation)</b>	$H_2O_2 + O_2^{\cdot -} \rightarrow \cdot OH + OH^- + O_2$
(v) <b>Reaction of H<sub>2</sub>O<sub>2</sub> with electrons (conduction band electrons are generated from semiconductor photocatalyst under UV irradiation UV + hydrogen peroxide + ozone)</b>	$H_2O_2 + e^- \rightarrow \cdot OH + OH^-$ $O_3 + OH^- \rightarrow \cdot OH$ $3O_3 + h\nu \rightarrow 2\cdot OH$ $H_2O_2 + h\nu \rightarrow 2\cdot OH$ $H_2O_2 + O_3 \rightarrow 2\cdot OH$
<b>Ozone + sonolysis</b>	$H_2O \rightarrow \cdot OH + OH^-$ $H_2O \rightarrow (1/2)H_2 + (1/2)H_2O_2$ $H_2O_2$ $O_3 \rightarrow O_2(g) + O(^3P)(g)$ $O(^3P)(g) + H_2O(g) \rightarrow 2\cdot OH$

water which is not suitable for usage in day to day life of human beings. As a result of the usage of polluted water, water borne diseases spread throughout the world and in the worst case it causes the mortality of children [4,5]. Naturally available drinking water is rare and limited nonetheless it is needed for all domestic and commercial applications which clearly illustrates how even a small shortage of water could become a threat to mankind. In day to day life, the environmental pollution is appears to be very much responsible for the negative consequences in the lives of all beings on the earth. The ingestion of chemical substances into the water bodies by the consumers destroys the quality of water continuously, which is called aquatic pollution. The contaminating (foreign) substances are generally classified into organic and non-organic contaminants, while Adewuyi classifies the contaminating pollutants into various categories [6]. The discharge of the un-mineralized contaminants, for example effluents released from the textile industries, pulp and paper industries, pharmaceutical industries etc., into the water resources causes environmental pollution. Similarly, non-organic substances, for example, excessive addition of agricultural chemicals causes water as well as land pollution [7]. The release of these un-neutralized pollutants into the environment creates detrimental effects and adulteration of these chemicals into the water bodies not only creates health hazards to the human beings but also affects the aquatic organisms. For example the presence of 4-nonylphenol (endocrine disrupter) in sewage disposal plants creates the feminizing effects in fishes which is a serious problem in terms of ecological conservation [8–10].

To avoid the hazardous effects created by the presence of these chemicals, many methodologies such as adsorption [11], biodegradation [12,13], photocatalysis [14] and ozonation [15] are proposed one by one from the early 1970s for the initiation of degradation of environmental pollutants [16–18]. As a result of these innovations, some awareness has been created among the public by the researchers about environmental pollutants. Many research groups have started working towards the complete removal of these pollutants from the environment by proposing, developing and adopting the new technologies for the degradation

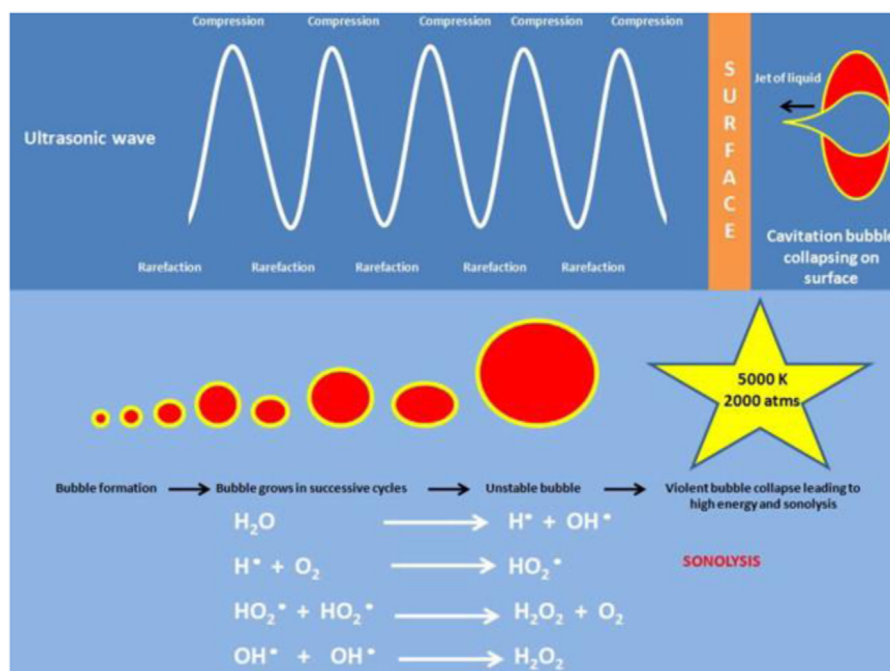


**Fig. 1.** Generation of an acoustic bubble [39].

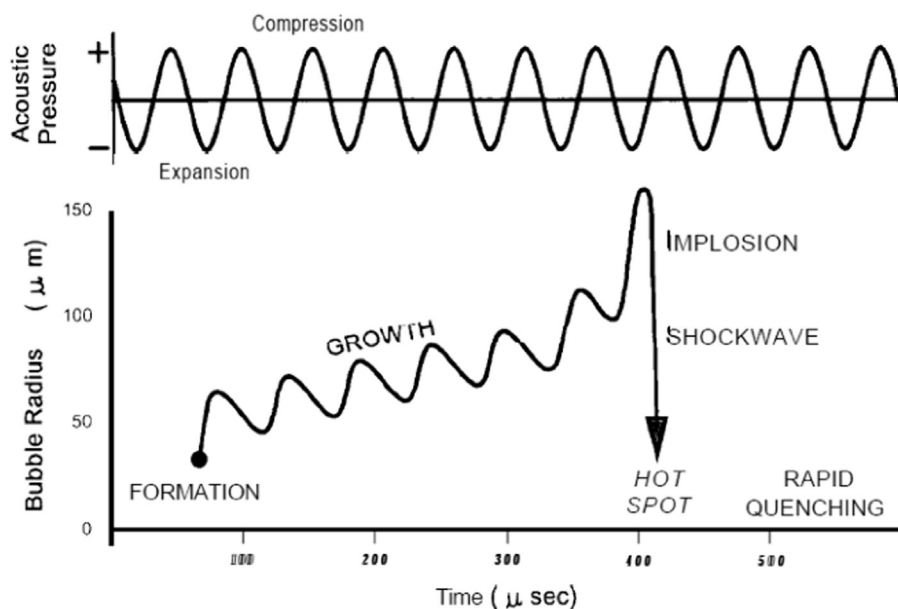


Fig. 2. Transient cavitation [40].

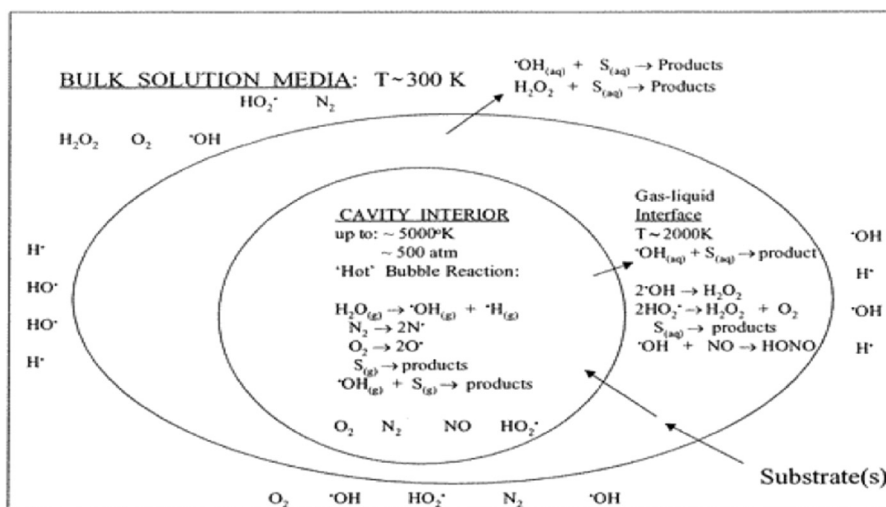


Fig. 3. Three reaction zones in the cavitation process [6].

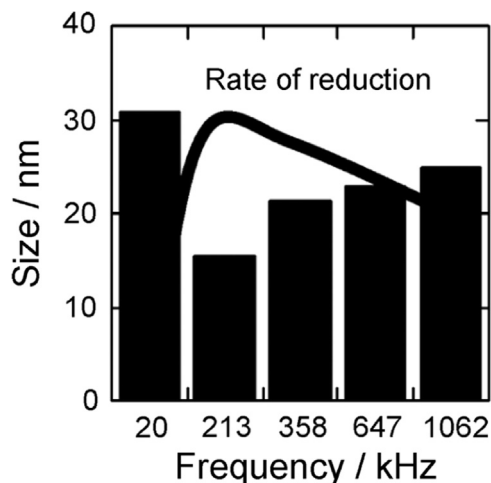


Fig. 4. Effect of ultrasound frequency on the sonochemical synthesis of gold nanoparticles [60].

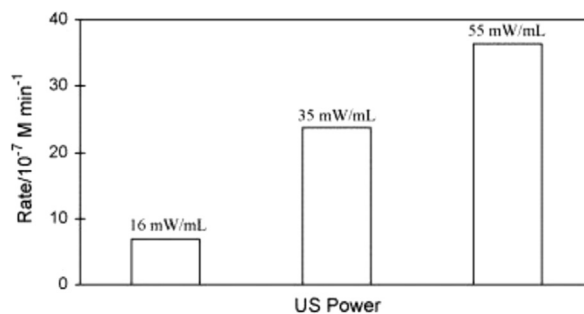


Fig. 5. Effect of ultrasound power on the degradation rate of monocrotophos [67].

of environmental pollutants, and few of them were tabulated in Table 1 [19,20]. Among the various methodologies developed for the degradation of environmental pollutants, advanced oxidation processes (AOPs) are more effective for the complete removal of a wide variety of contaminants [21–23]. AOP is nothing but the complete mineralization of various pollutants: the term

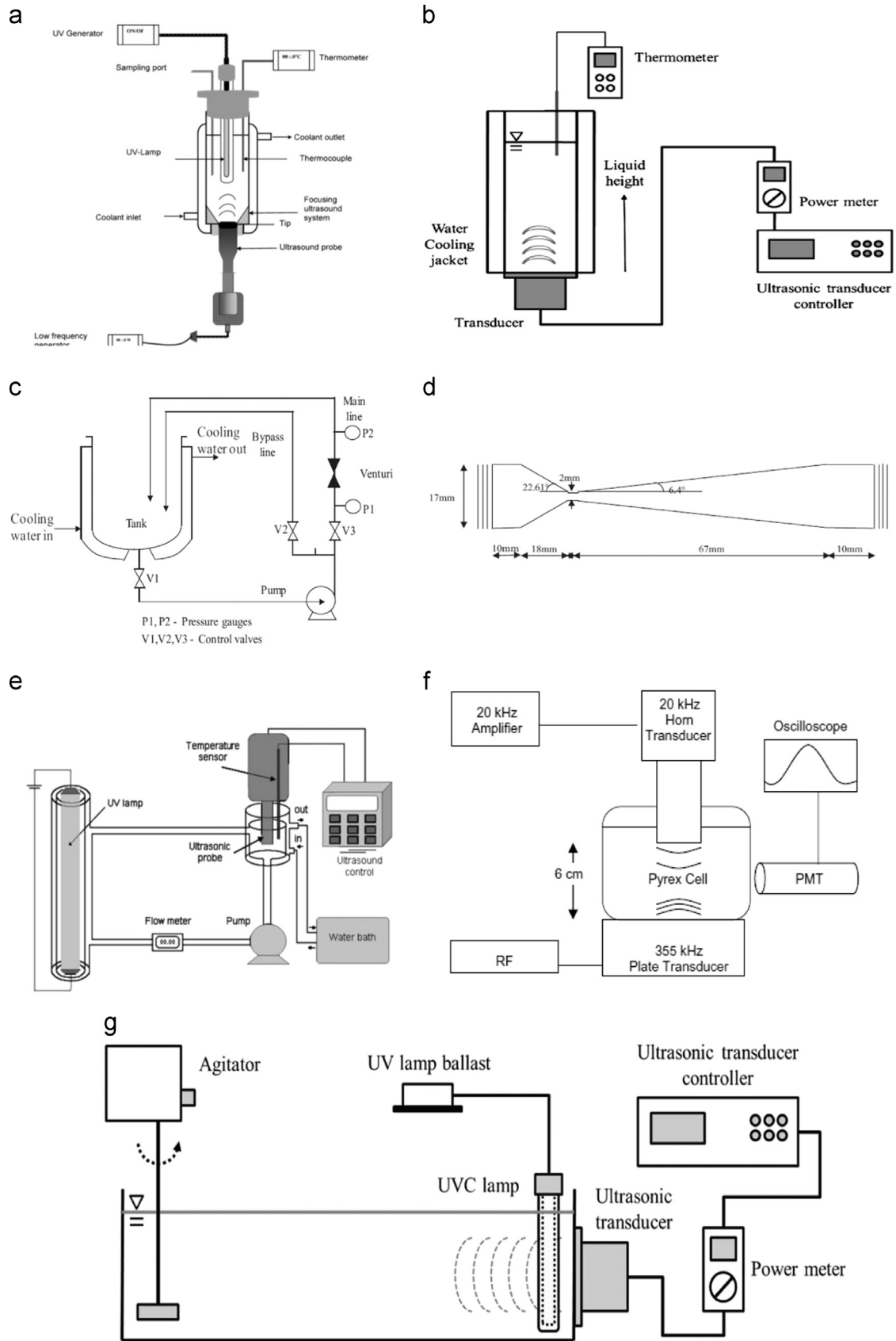


Fig. 6. Various available geometries of reactors for ultrasound-assisted photocatalysis [86–90,99].

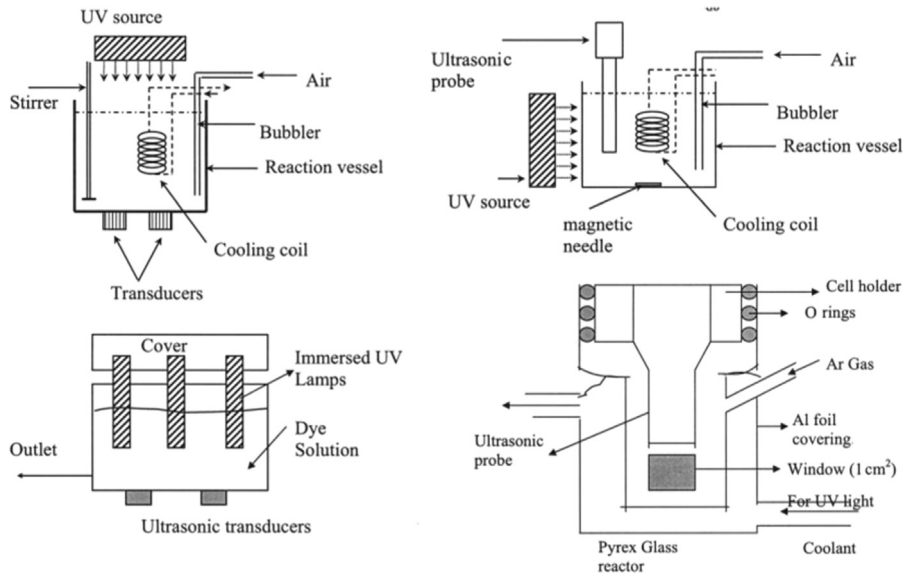


Fig. 7. Typical schemes for the sonophotocatalytic batch reactors [238].

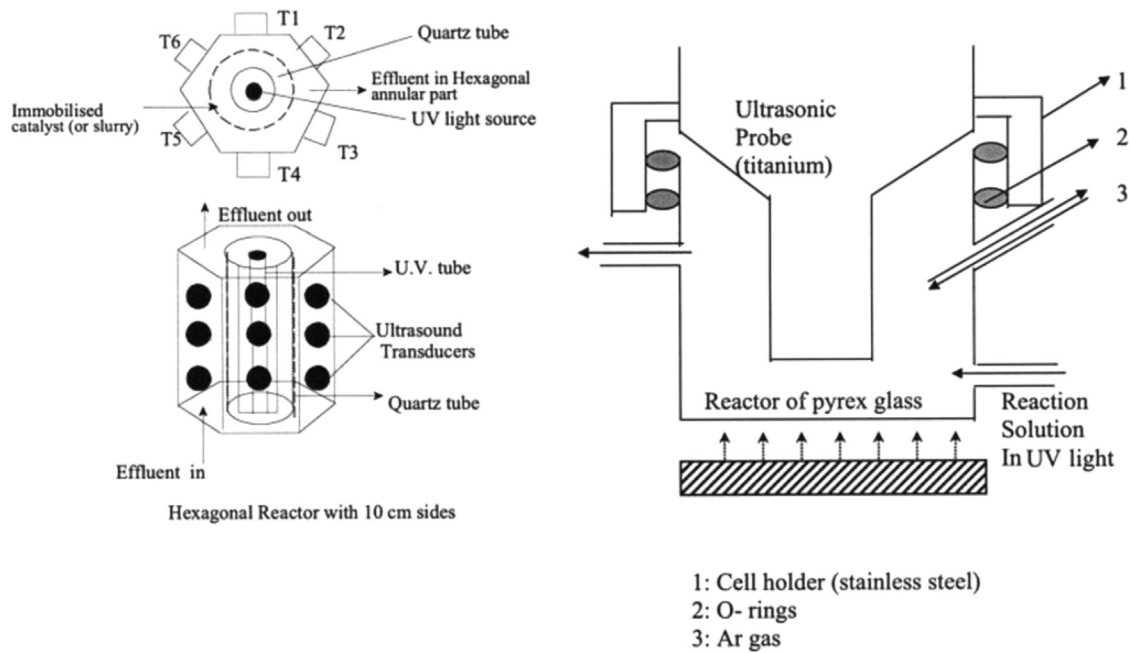


Fig. 8. Typical schemes for the sonophotocatalytic continuous reactors [238].

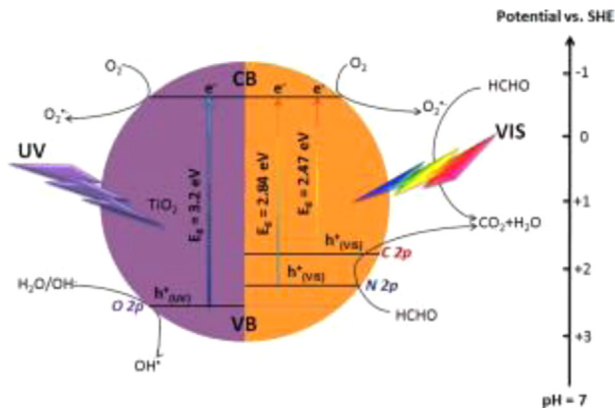


Fig. 9. The ultraviolet and visible light assisted electronic excitation of semiconductor nanoparticles [127].

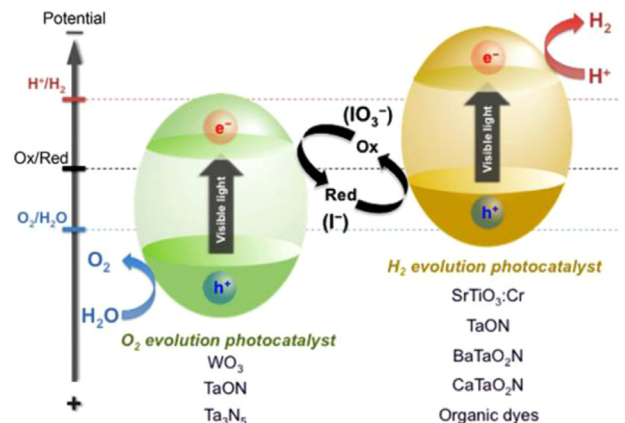


Fig. 10. Overview of water splitting on Z-scheme photocatalysis system [130].

mineralization suggests the conversion of pollutants into carbon dioxide, water and mineral acids by the oxidation process. Some of the important innovations that are readily applicable in large scale are the AOPs (Table 1) involving  $O_3/H_2O_2$ ,  $Fe^{2+}/H_2O_2/Fe^{3+}$ ,  $UV/O_3$ ,  $UV/H_2O_2$ ,  $UV/O_3/H_2O_2$ , catalytic ozonation, sonolysis, photocatalysis, and combined sonophotocatalysis [24–34]. The combination of these AOPs has received much interest from the environmental remediation research communities. The combined AOPs were employed to study the degradation of environmental pollutants: alternatively the AOPs coupled with sonolysis technique have received much interest and it may be applicable for the degradation of a wide variety of organic contaminants [34–38]. The following are the combination of AOPs with sonolysis technique, sonophotocatalysis (sonolysis coupled with photocatalysis), sono-Fenton (Fenton), Sonophoto-Fenton (photo-Fenton) Sono-electro-Fenton (electro-Fenton) and sonolysis coupled with ozonolysis. In this review we are presenting and discussing some of the recent innovations involved in the mineralization of various environmental contaminants by using sonochemical and combined sonochemical oxidation techniques.

## 2. Sonolysis

The ultrasound generates the acoustic bubbles when it is passed through an aqueous medium which is called acoustic

cavitation as depicted in Fig. 1 [39]. The micro-bubbles produced during the acoustic cavitation will tend to increase and decrease its size continuously until the micro-bubbles reach the resonance size which is the mean size of the bubble before undergoing the violent explosion. After explosion the bubbles produce enormous

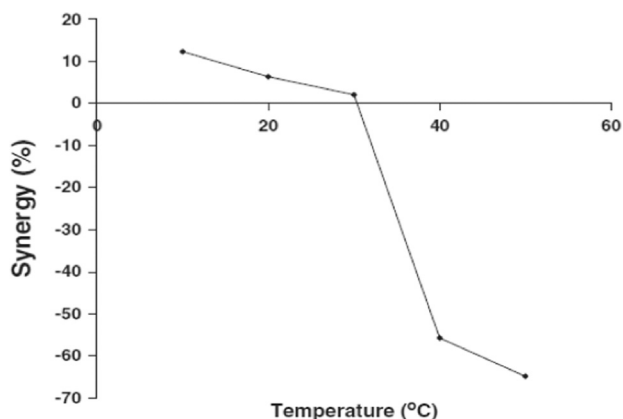


Fig. 11. Relationship between synergistic, additive and antagonistic effects as a function of the solution temperature [174].

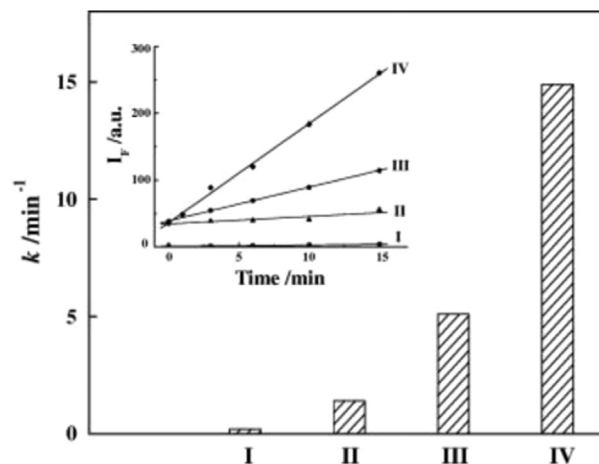


Fig. 12. Rate constants for the generation of  $\bullet OH$  radicals in the systems of (I)  $US-Fe_3O_4$ , (II)  $H_2O_2-Fe_3O_4$ ; (III)  $US-H_2O_2$ ; and (IV)  $US-H_2O_2-Fe_3O_4$ . The inset gives the kinetics of  $\bullet OH$  generation in the four systems [176].

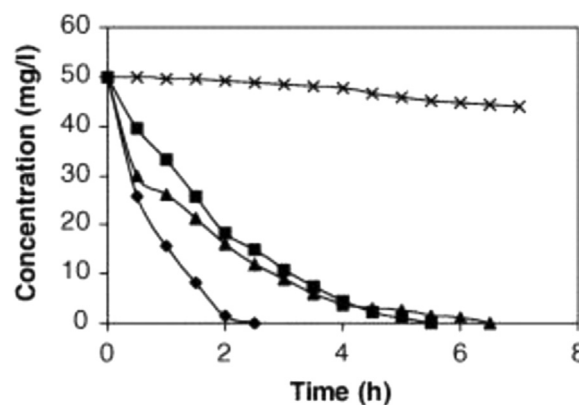


Fig. 13. Effect of radical quenchers on the degradation rate under sonophotocatalytic conditions: (x) 1,4-benzoquinone, (■)  $NaN_3$ , (+) DABCO, (◆) no quencher, (dye)=50 ppm,  $(TiO_2)=300$  mg/l, (quencher)=100 mg/l [177].

Table 2  
Rate constants of TCP degradation by sonolysis, photolysis and sonophotolysis [174].

Temperature (°C)	Degradation process	Rate constant (h <sup>-1</sup> )	R <sup>2</sup>	Synergy (%)	Synergistic effect
10	Sonolysis	0.0131	0.9746	(+ )12.22	Synergistic
	Photolysis	0.0027	0.8718		
	Sonophotolysis	0.0180	0.9036		
20	Sonolysis	0.0268	0.9768	(+ )6.45	Synergistic
	Photolysis	0.0080	0.7949		
	Sonophotolysis	0.0372	0.9046		
30	Sonolysis	0.0603	0.9764	(+ )1.92	Almost additive
	Photolysis	0.0416	0.9900		
	Sonophotolysis	0.1039	0.9946		
40	Sonolysis	0.1445	0.9793	(– )55.79	Antagonistic
	Photolysis	0.1417	0.9925		
	Sonophotolysis	0.1837	0.9866		
50	Sonolysis	0.2397	0.8974	(– )65.01	Antagonistic
	Photolysis	0.2347	0.9864		
	Sonophotolysis	0.2875	0.9970		

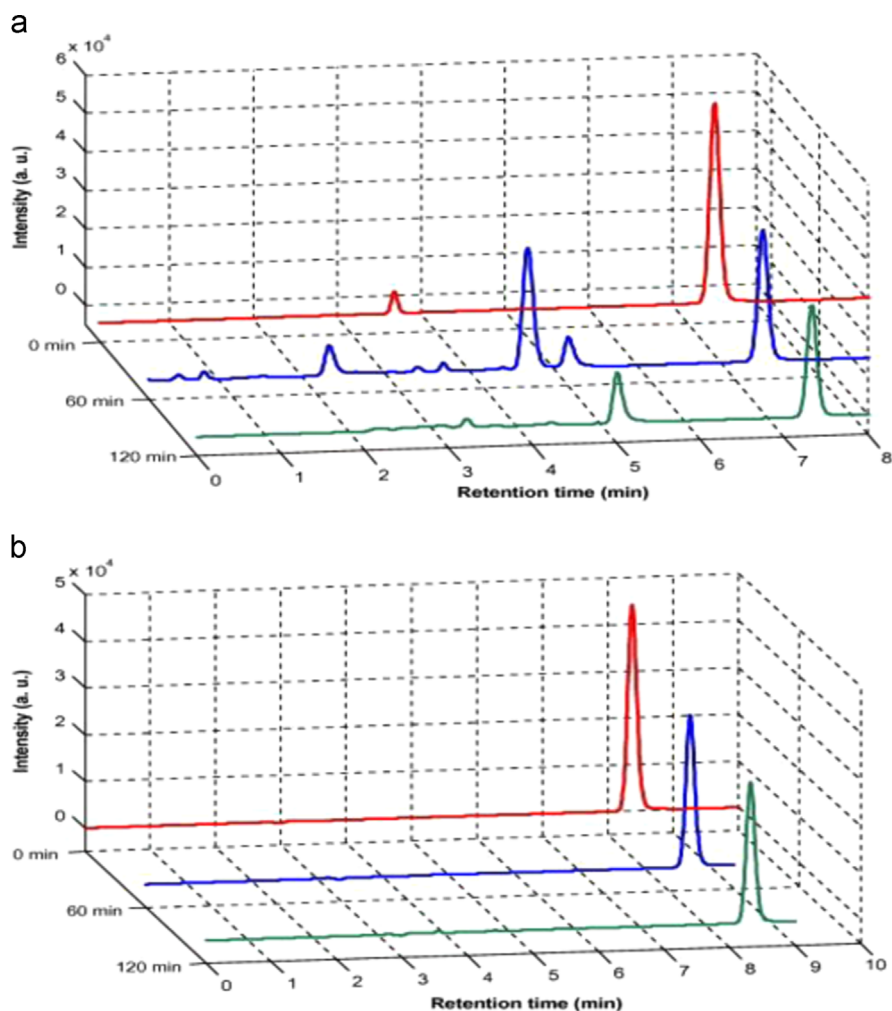


Fig. 14. HPLC spectra of 4-CP degradation against reaction time: (a) sonolysis and (b) sonophotocatalysis [179].

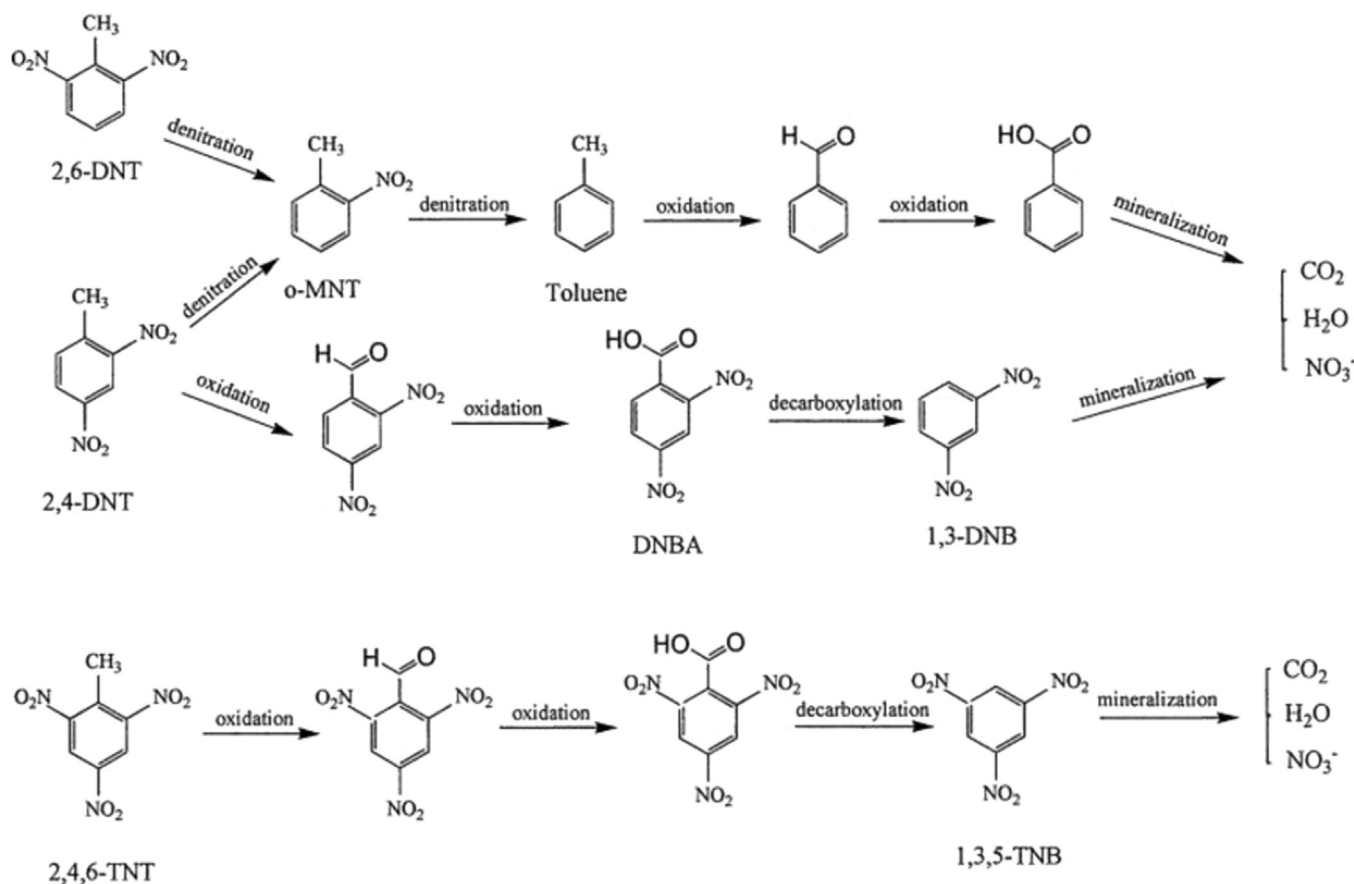
amount of heat, pressure and various free radicals within the aqueous medium [40–43]. The time-profile for the violent explosion during acoustic cavitation is shown in Fig. 2. Both Figs. 1 and 2 are obliging to explain the phenomenon of impulsive explosion of bubbles. The collapse of these bubbles can produce an enormous number of radicals (primary) which are responsible for the synergetic effect. The bubbles were also referred to as micro-reactors or hotspots (Fig. 2), since they are acting as the center for the occurrence of chemical reactions. During the acoustic cavitation light will be emitted due to the bubbles collapse called sonoluminescence (SL) and sonochemiluminescence (SCL) [44–47].

Numerous theories have been proposed to explain the phenomenon of acoustic cavitation [48–54]: among the theories proposed “hot spot theory” (Fig. 2) has given the satisfactory explanation. The presence of dissolved gas, substances and other materials situated near the hotspots are responsible for the generation of highly reactive primary radicals which will further produce the secondary radicals during the acoustic cavitation [42,55,56]. In addition to that the production of enormous amount of heat during the acoustic cavitation helps the pollutants to undergo pyrolysis if the pollutants are volatile in nature. The three reaction zones and the production of high temperature, pressure and free radicals during the process of sonolysis (Fig. 3) have been discussed more in detail with the necessary examples in the cited references [6,42,57].

### 2.1. Factors influencing acoustic cavitation

The various parameters involved in the sonochemical reactions determine the efficiency. Thus the various parameters involved in the sonochemical reactions should be discussed before talking about the combined sonolysis with other AOPs. The ultrasound frequency applied during the sonochemical reaction plays a major role in production of micro-bubbles and radicals during the acoustic cavitation. In the literature, the effect of ultrasound frequency from 20 kHz to 1056 kHz had been studied [58–61] to find the optimum ultrasound frequency for the sonochemical reactions (Fig. 4). The application of minimum ultrasound frequency (20 kHz) on the sonochemical reactions was found to produce less number of active bubbles which were required for the sonochemical reactions. However, 1056 kHz ultrasound frequency results in the production of less number of active radicals due to the production of high number of colliding bubbles, primary radicals and the compression cycle occurs faster than the time required for the microbubbles to collapse. In the case of minimum ultrasound frequency, it is not sufficient for the active bubbles production due to relatively higher amount of water vapor present inside the collapsing bubbles. The optimized ultrasound frequency for the effective cavitation is 200–600 kHz since this range of ultrasound frequency produces a large number of active bubbles and radicals during the acoustic cavitation. Moreover, Drijvers et al. [62] have reported that 520 kHz is more energetically efficient to carry out the sonochemical reactions





**Scheme 1.** Plausible reaction pathways of DNTs and 2,4,6-TNT in wastewater under ultrasonic irradiation [182].

in aqueous medium. The ultrasound power (amplitude) provided during the acoustic cavitation has also a positive influence on the sonochemical reactions (Fig. 5). If the supply of ultrasound power to the sonochemical reaction is increased the rate of the reaction was found to increase continuously [32,63–67] up to a certain limit and further increase in the acoustic power leads to decrease in the rate of the reaction. Nevertheless there is no report available in the literature about the optimum acoustic power at a particular ultrasound frequency which is to be applied in the sonochemical reactions.

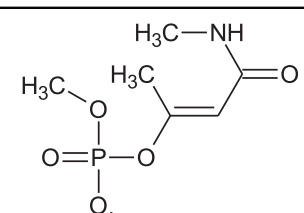
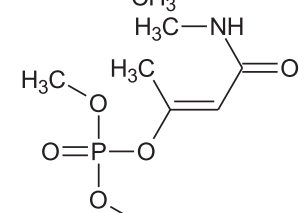
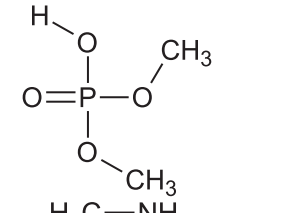
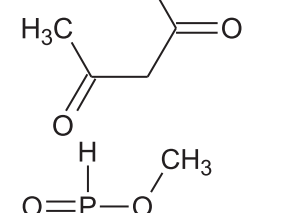
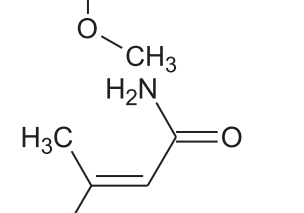
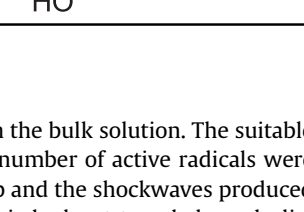
The effect of solvents on the sonochemical reactions was investigated by Lorimer and Mason [68]. They have reported that higher number of effective cavitation occurred when high viscous liquid was used as the solvent whereas in the case of diethyl ether (solvent for the cavitation process), bubble production was inhibited or stopped [69]. Further, the characteristics of the solvents such as surface tension, vapor pressure etc., decide the efficiency of the acoustic cavitation. The application of ultrasound irradiation has been extended to synthesize nanoparticles, nanocomposites and nanomaterials in the recent past [70–81]. In the literature it is found that most of the nanomaterials synthesize was reported by the sonochemical reactions containing the polymer substances (for example PVP, PEG, etc.) along with the precursor solutions. The polymer materials added to the substance protect the nanomaterials from aggregation and the presence of polymer molecules indirectly increases the viscosity of the solvents and effective cavitation can be achieved due to the presence of these polymer molecules [70–72]. Therefore before carrying out an ultrasonic irradiation the suitable features of the solvents are to be kept in mind since these properties can alter the yield of the acoustic cavitation or sonochemical reactions.

In addition to these parameters, the operating temperature and pressure of the sonochemical reactions can modify the yield in the reactions. The parameters temperature and pressure of the sonochemical system are inversely proportional to each other; for example increase in temperature (at constant pressure) leads to decrease in the rate of the sonochemical reaction [82,83]. Similarly, as the pressure (at constant temperature) is increased the rate of the reaction was dramatically increased [84,85]. The possible reason for the observed behavior is due to the alteration in vapor pressure of the liquid (solvent) which has the direct influence on the sonochemical reactions. The optimized temperature and pressure give more favorable results in the sonochemical reactions. The role of other parameters involved in the sonochemical reactions has been discussed elsewhere [6].

### 3. Geometry of sonochemical reactors for the enhanced degradation of environmental pollutants

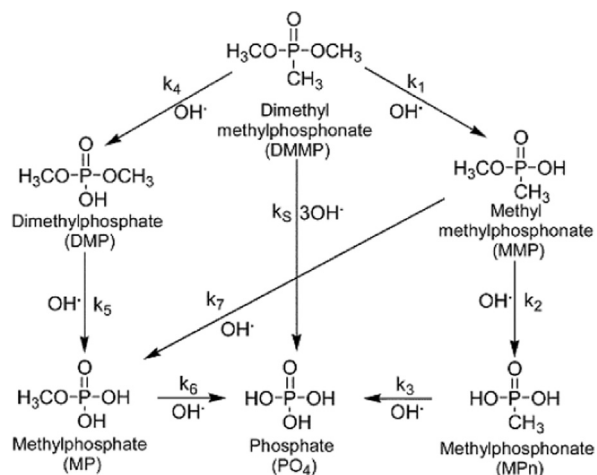
The geometry of the sonochemical reactors plays the major role in deciding the yield of the sonochemical reactions [86–90], which further enhances the degradation of environmental pollutants in addition to the parameters discussed in Section 2.1. The hydrogen peroxide produced during the sonochemical reactions will harvest the surplus number of powerful non-selective hydroxyl radicals [91,92], which depends on the geometry of the sonochemical reactors [93]. If the production of H<sub>2</sub>O<sub>2</sub> exceeds a particular concentration, rate of the sonochemical reaction decreases dramatically due to hole-scavenging effect [93–96]. Recently, Ashokkumar [97] has reported that the sonochemical oxidation reactions involving 20 kHz sonohorn in the degradation of organic contaminants results in the contaminants near to the tip of the horn

**Table 3**  
Sonolytic, photocatalytic and sonophotocatalytic degradation products of MCP using TiO<sub>2</sub> [67].

S. no	m/z	Formula
1	223	
2	208	
3	127	
4	115	
5	111	
6	101	

getting more oxidized than those in the bulk solution. The suitable reason for the observation is high number of active radicals were produced near to the edge of the tip and the shockwaves produced during the phenomenon of sonolysis had not traveled much distance from the horn. The radicals produced from the shock waves react more with the nearest molecules (contaminants) and thus the radicals cannot propagate throughout the solution. The various number of sonochemical reactors in practice are presented in Fig. 6.

The geometry of the sonochemical reactors has conservative influence on the sonochemical reaction yields, for example 92.9% and 98% removal of Rhodamine-B was achieved by Ahmedchekkat et al. [90], Mishra and Gogate [98] respectively using 7 L geometry of hydrodynamic cavitation setup. Saharan et al. [99,100] have achieved the maximum degradation for Acidred 88 and Reactive



**Scheme 2.** Dimethyl methylphosphonate (sono) photocatalytic oxidation [184].

red 120 with 15 L geometry of hydrodynamic cavitation setup as shown in Fig. 6(c,d). Some of the novel sonochemical reactor geometries which were developed for the large scale applications are shown in Figs. 7 and 8 proposed by Gogate and Pandit [93] for the degradation of environmental contaminants. The detailed energy consumption and operational methods and the advantages of the sonochemical reactor geometries were discussed elsewhere by Gogate and Pandit [93].

#### 4. Combined sonophotocatalytic degradation of environmental pollutants

##### 4.1. Photocatalysis

General classification of photocatalysis is homogeneous and heterogeneous. The degradation of organic contaminants, volatile compounds and microorganisms had been carried out in the presence of ultra-violet (UV) light during the past few decades [101–111]. To improve the overall efficiency, oxidizing agents were added to enhance the rate of the degradation process which includes Fe<sup>2+</sup>/Fe<sup>3+</sup>/H<sub>2</sub>O<sub>2</sub> photocatalysis. However, the remediation of the wastewater by homogeneous catalysis is not recommended since the metal ions have their notorious impact on the aquatic environment [30,31]. The other type is heterogeneous photocatalysis, in which many of them are photochemical processes that are based on photoinduced electron transfer processes [106–111]. To overcome the drawbacks of conventional treatment methods for the degradation of environmental pollutants, heterogeneous photocatalysis has been proposed by many scientists and engineers [14,101–120]. The photocatalysis technique is to be adopted for the degradation of contaminants which generally includes semiconductor as the photocatalyst [121,122]. In photo-generated catalysis the activity depends on the ability of the catalyst to create the electronic charges, free radicals which can undergo the secondary reactions. The essential condition for the photocatalytic degradation is its Gibbs free energy change should be negative ( $\Delta G^\circ = -ve$ ); if the reaction's Gibbs free energy change becomes positive ( $\Delta G^\circ = +ve$ ) then the reaction is called photosynthesis [123–126].

Heterogeneous photocatalysis can be generally categorized into the following three types namely, catalyzed photolysis, semiconductor sensitization and dye sensitized photocatalysis. Semiconductor materials namely titanium dioxide, zinc oxide and other nano-structured semiconductor materials undergo the band gap excitation under UV as well as visible light irradiation, yielding the

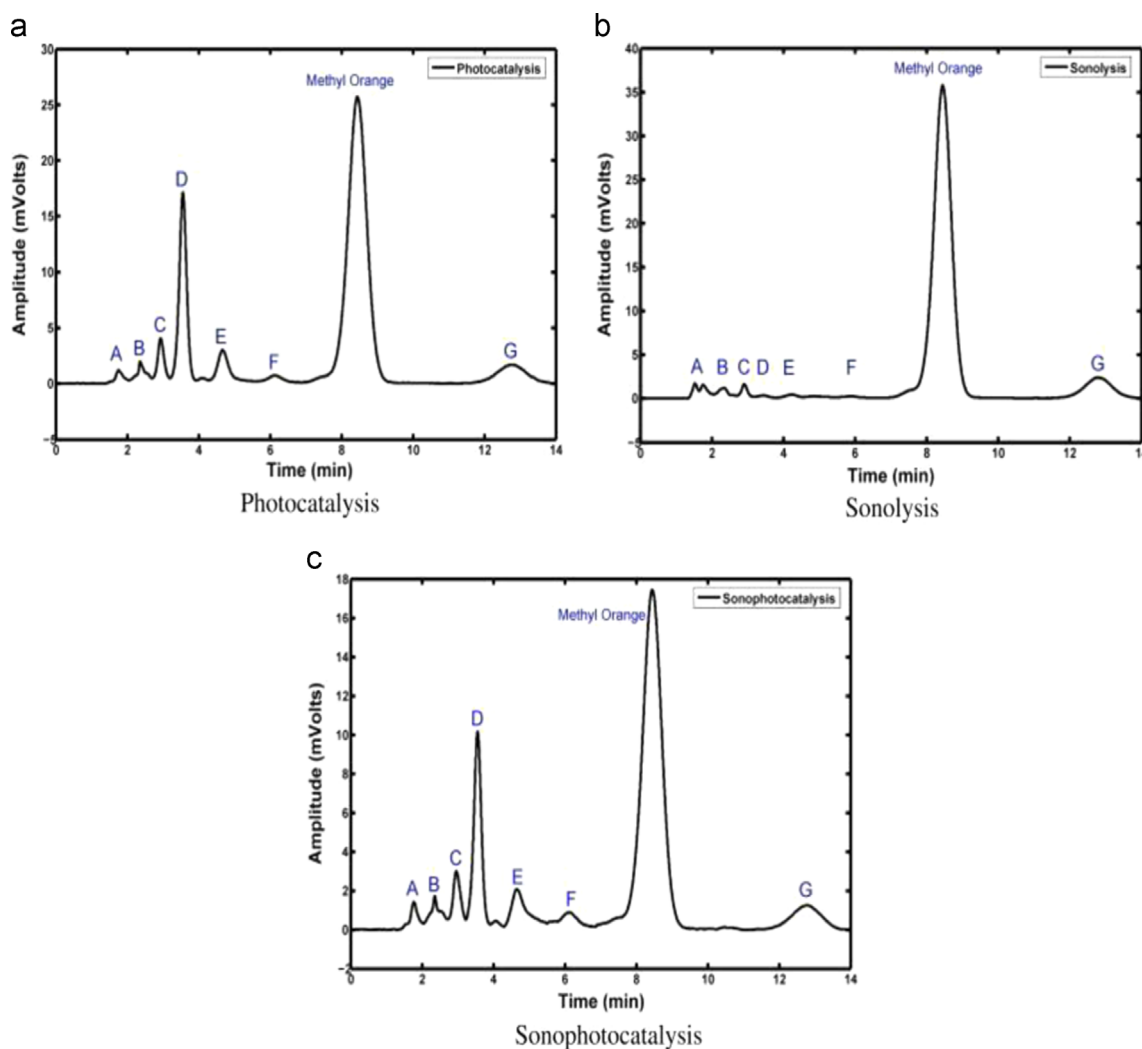


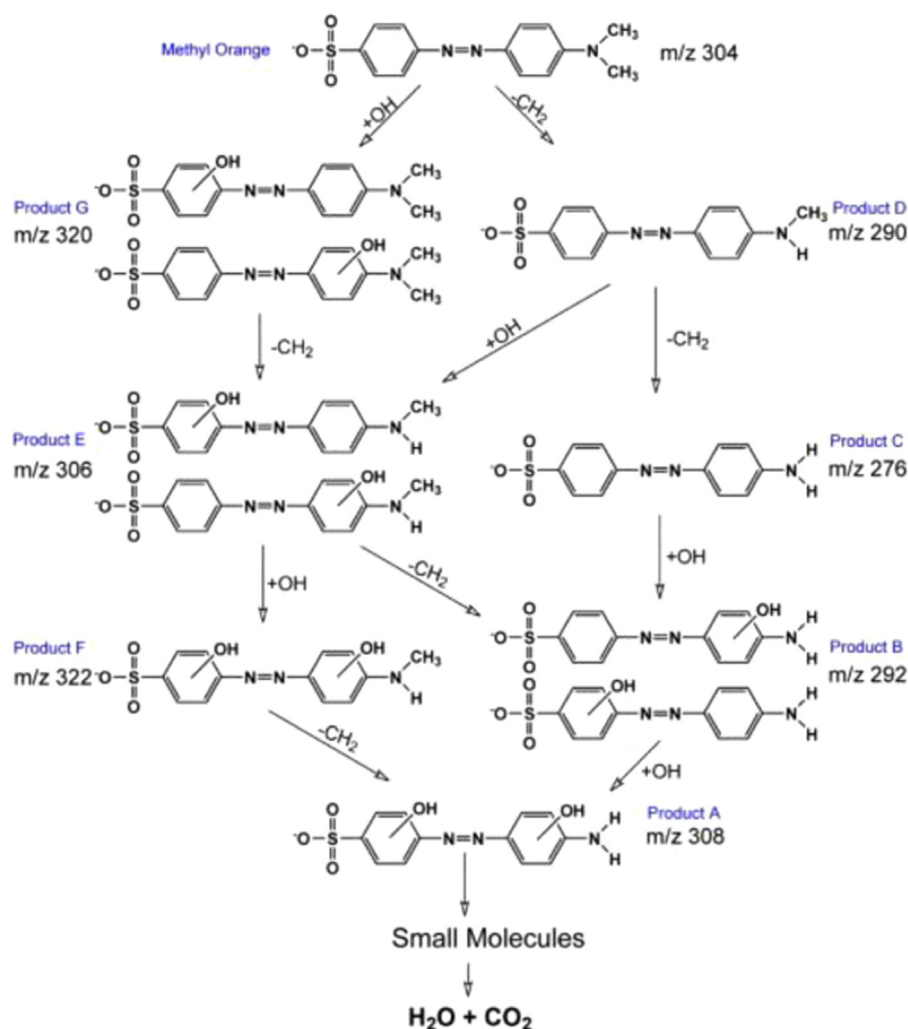
Fig. 15. HPLC plot observed after 60 min of photocatalytic, sonolytic and sonophotocatalytic degradation of methyl orange in the presence of  $\text{TiO}_2$  [175].

electronic charges namely electrons ( $e^-$ ) and holes ( $h^+$ ) (Fig. 9) [127]. The rapid recombination of the electronic charges reduces the efficiency of the over-all process. Therefore the recombination can be prevented by the addition of electron and hole acceptors. The formation, recombination and prevention of electronic charges have been reviewed well in the recent past and much of the early investigations and fundamentals of photocatalysis have been summarized elsewhere [101–111].

Most of the fuel, electrical and chemical demands of the human beings can be fulfilled by using the available sunlight on the earth surface [128,129]. The availability of sunlight on the earth surface is  $\sim 1000 \text{ W m}^{-2}$  which is not utilized appropriately so far. Therefore the development of methodologies towards the proper utilization of available sunlight on the earth surface will solve the demands. One such method is the development of photocatalysts which can harvest the maximum portion of visible (sun) light and degrade the contaminants. The process of visible light excitation of the photocatalysts (Fig. 9) makes the photocatalysis process cheaper and avoids the usage of UV light as the source for photoexcitation processes. Similarly visible light assisted photocatalysis which can be utilized for the production of “green fuel” (Fig. 10), which is another important topic for discussion. The recent reviews appeared in the area of visible light assisted hydrogen production have been directed for future studies [39,130–132].

Due to the very low or no absorption in the visible region, semiconductor photocatalysts such as  $\text{TiO}_2$  and  $\text{ZnO}$  cannot efficiently harvest the maximum portion of solar energy. Therefore, constant efforts have been made to enhance their efficiency. Two major drawbacks of any individual large band gap semiconductor identified are the recombination of electronic charges (electron and holes) and limited light harvesting ability. These are the limiting factors in the economical usage of the semiconductor photocatalysts. The former can be minimized by using metal nanoparticles on the semiconductor, as metal functions as sink for the electron and decreases the recombination of electronic charges. Sensitization with dyes is one of the most commonly used methods to overcome the limited light harvesting ability of the large band gap semiconductors. The photocatalytic degradation is highly pollutant specific. The rate of photodegradation depends on the surface and structural properties of the nano-size catalysts, and the parameters like pH, concentration of catalyst, pollutants, oxidants, etc., To overcome these problems associated with the usage of semiconductors as visible light active photocatalysts much effort has been made by our research group for the degradation of various environmental pollutants in the presence of various nanocatalysts [94–96,133–150].

Recently certain new and novel promising photocatalysts have been reported in the literature for the degradation of environmental pollutants [151–158]. Most of the semiconductor materials are visible light inactive since the band gap is very high, in other



**Scheme 3.** Schematic illustration of the proposed degradation pathway and the events taking place during the sonophotocatalytic degradation of MO [175].

words high energy is required for the band gap excitation. Alternatively the low band gap semiconductors as photocatalysts are experiencing the photocorrosion instead of catalyzing the photooxidation of organic contaminants [158–164]. The researchers have developed the integrated semiconductor nanocatalysts to produce the visible light active as well as photochemically stable photocatalysts; for example Arai et al. [165] and Anandan et al. [137] have reported the synthesis and applications of  $\text{CuBi}_2\text{O}_4/\text{WO}_3$  and  $\text{Bi}_2\text{CuO}_4$  nanocomposite catalysts. The combination of various semiconductors produce the hybrid nanocomposite materials for the different applications. Alternatively, Liu et al. [166] and Manivel et al. [167] have developed the heterojunction p–n type semiconductor nanocatalysts to avoid the drawbacks of the semiconductor photocatalysis. In addition to that  $\text{BiOCl}$ ,  $g\text{-C}_3\text{N}_4/\text{TiO}_2$ , Metal Organic Frameworks (MOFs) are the novel and promising photocatalysts reported in the literature for the environmental purification [151–158].

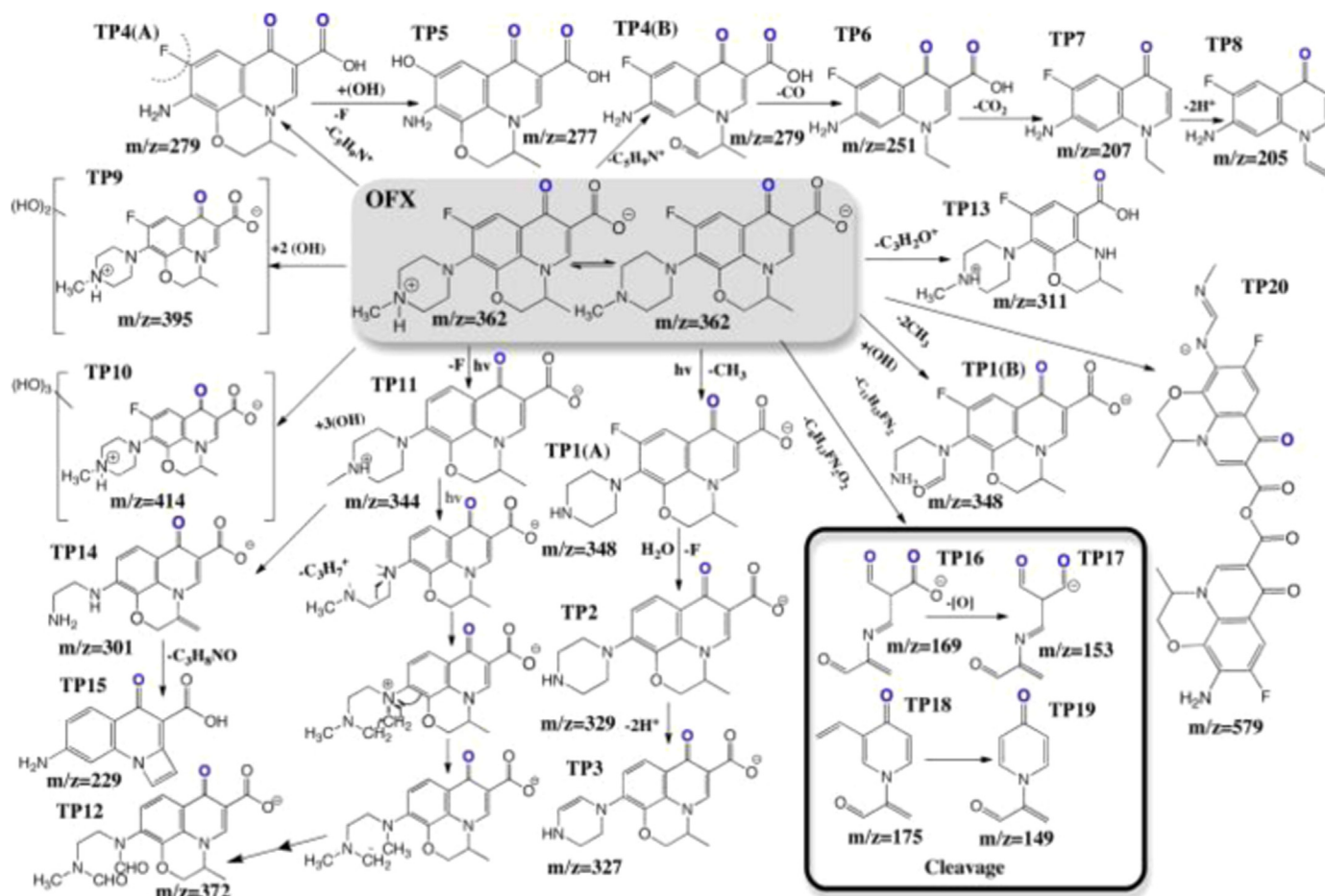
#### 4.2. Sonophotocatalysis

The sonophotocatalysis process can be defined as follows; the chemical degradation of environmental pollutants by the photoacceleration of semiconductors in the presence of ultrasound irradiation [168–171]. According to the classification of Joseph et al. [19], the term sonophotocatalysis includes the various AOPs such as (i) Photolysis; (ii) Photocatalysis; (iii) Sonolysis; (iv)

Sonocatalysis and (v) Sonophotolysis. The combination of these AOPs produces the sonophotocatalysis reactions i.e., the degradation of environmental pollutants by passing the ultrasound and light through the semiconductor existing in aqueous medium (known as acoustic cavitation). The band gap excitation of the semiconductor as well as the production of acoustic bubbles during the sonophotocatalytic degradation are directing the sonochemical reactions. The main aim of the combination of these two AOPs is to reduce the operational cost and time duration of the degradation process. Therefore, sonophotocatalysis is expected to be more energetically and economically efficient which can be calculated by using Eq. (1). From the equation, we can calculate the synergetic effect and additive effect for the degradation of various environmental pollutants which indicates the influence of the various parameters involved in the sonophotocatalytic reactions as we discussed in the earlier Sections 2 and 3.

$$\text{Synergy} = \frac{k_{\text{sonocatalysis}} + k_{\text{photocatalysis}}}{k_{\text{sonophotocatalysis}}} \quad (1)$$

Sonocatalysis means that ultrasound can be employed as the alternative source of photoirradiation for the semiconductor catalysts. Sonolysis of the semiconductor solution induces the holes from the valance band of semiconductor to react with the environmental pollutants adsorbed near to the valance band [172]. The sonoluminescence produced during the process of sonolysis can assist the sonocatalytic degradation of pollutants through the band



Scheme 4. Proposed reaction pathway for the photodegradation of ofloxacin in secondary treated effluent [185].

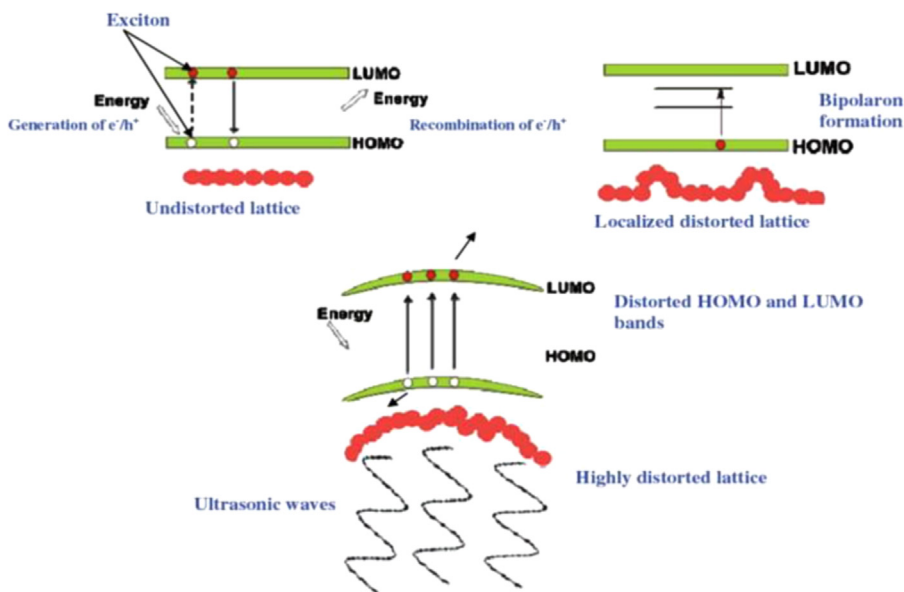


Fig. 16. Behavior of polymeric organic semiconductor as a photocatalyst under ultrasonic irradiation [191].

gap excitation [173]. The mechanistic pathway of sonocatalysis is not well established so far; however the further research in this direction can give the clear knowledge about the mechanism, holes migration and the role of electrons involved in the sonocatalysis process.

Joseph et al. [174] have calculated the synergy of the combined AOPs by following Eq. (2), the combined sonolysis and photolysis of the degradation (in the absence of catalysts) of 2,4,6-trichlorophenol (TCP). The authors have shown the experimental correlation between the temperature and the synergy of the

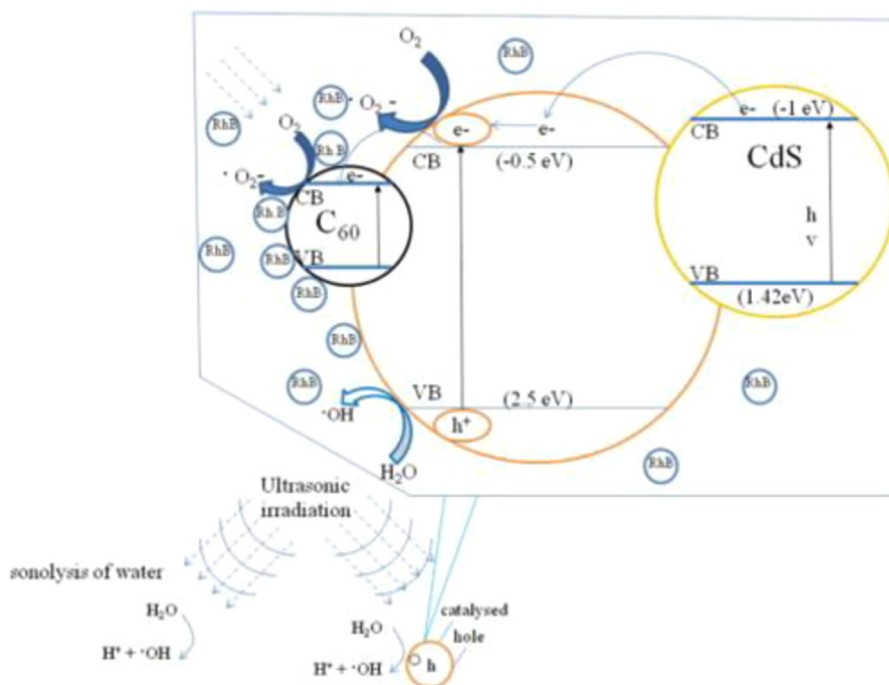
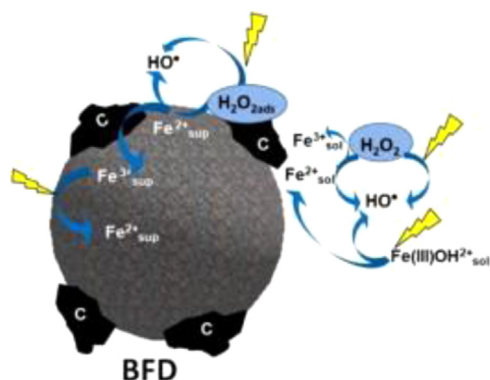


Fig. 17. Schematic drawing of separation of generated electrons and holes on the interface of CdS-C60/TiO<sub>2</sub> compounds under ultrasonic irradiation [173].



Scheme 5. Some reactions involved in advanced oxidation processes [218].

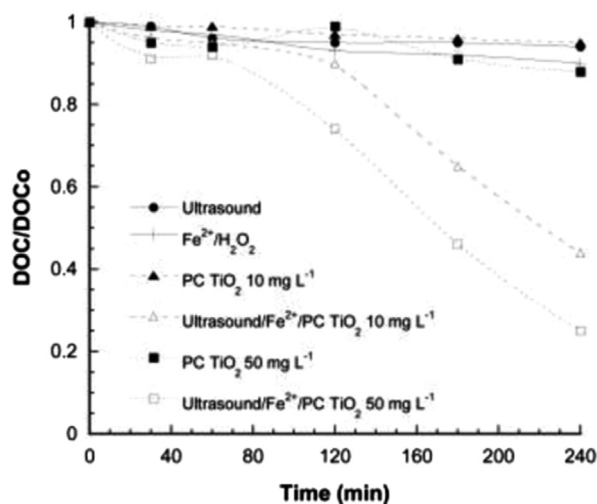
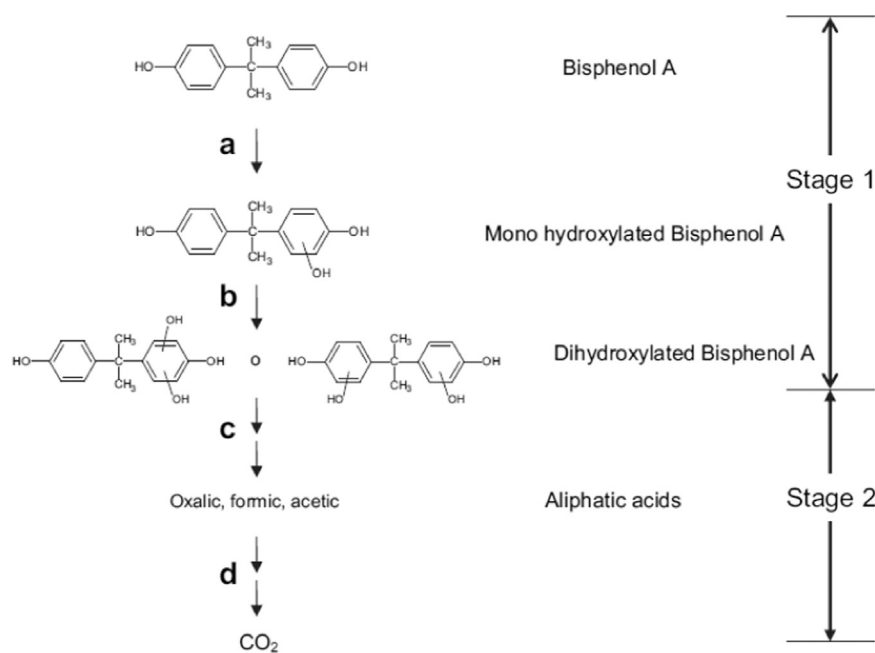


Fig. 18. DOC elimination by ultrasound, TiO<sub>2</sub> photocatalysis (PC), photo-Fenton and combined ultrasound/Fe<sup>2+</sup>/TiO<sub>2</sub> photoassisted processes applied to solutions saturated with oxygen [219].

degradation processes (Fig. 11 and Table 2). The reactions are termed as additive, synergetic and antagonistic if the synergy values calculated from Eq. (2) are zero, positive and negative respectively. The experimental data (Fig. 11 and Table 2) clearly illustrate the relation between the temperature and yield of the sonochemical reactions which supports our earlier discussion about the role of temperature in the sonochemical reactions. The negative synergy has also been reported by He et al. [175] in the case of sonophotocatalytic degradation of methyl orange.

$$\text{Synergy} = \frac{k_{\text{sonophotolysis}} - (k_{\text{sonolysis}} + k_{\text{photolysis}})}{k_{\text{sonophotolysis}}} \quad (2)$$

The quantity of effective free radicals produced during the ultrasonic irradiation enhances the efficiency of the processes. Wang et al. [176] has observed the synergetic effect on the degradation of Rhodamin B in the presence of magnetic Fe<sub>3</sub>O<sub>4</sub> nanoparticles and H<sub>2</sub>O<sub>2</sub>. The reason for the observed synergetic effect is due to the production of enhanced number of hydroxyl radicals during the sonication. The fluorescence technique was adopted to calculate the quantitative production of hydroxyl radicals, the results were represented in Fig. 12. Improved production of hydroxyl radicals was found in the system involving H<sub>2</sub>O<sub>2</sub>/nanocatalysts whereas in the absence of H<sub>2</sub>O<sub>2</sub> the hydroxyl radical production was found to be decreased. The formation of other intermediate species such as singlet oxygen (<sup>1</sup>O<sub>2</sub>) and superoxide (O<sub>2</sub><sup>•-</sup>) radicals during the visible light assisted sonophotocatalytic degradation of Reactive Red 198 has been examined by Kaur and Singh [177]. The investigation was carried out in the presence of various quenchers as shown in Fig. 13, 1,4-diazabicyclo [2,2,2] octane and 1,4-benzoquinone (100 mg/L) inhibited the sonophotocatalytic degradation of Reactive Red 198 which is due to the effective quenching of free radicals produced from the aqueous environment. The number of effective free radicals production and propagation to the bulk solution increases the efficiency of the sonophotocatalytic degradation. The degradation efficiency of the sonochemical reactions can be predetermined based on these techniques. The calculation before the sonochemical reactions helps the researchers to improve the efficiency of the degradation processes.



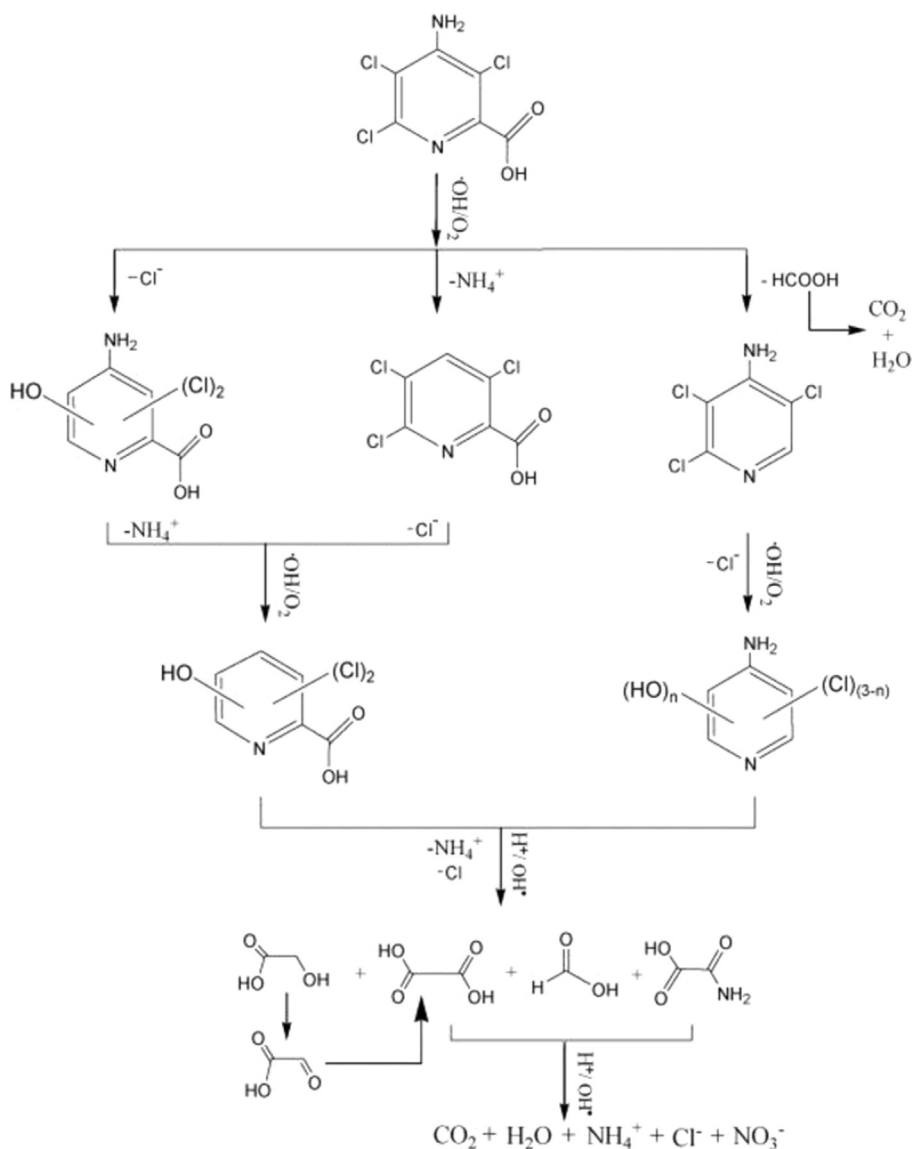
**Scheme 6.** Main steps during BPA degradation by ultrasound or photocatalysis [219].

Chang and Oh [178] have reported the sonophotocatalytic degradation of methylene blue (MB) in the presence of visible light active Fe/TiO<sub>2</sub>-MWCNT nanophotocatalysts. Madhavan et al. [32] have reported the sonophotocatalytic degradation of diclofenac in the presence of Fe-ZnO nanophotocatalysts. Neppolian et al. [179] have reported the visible light assisted sonophotocatalytic degradation of 4-chlorophenol (4-CP) in the presence of Bi<sub>2</sub>O<sub>3</sub>/TiZrO<sub>4</sub> nanoparticles. The various number of intermediates were identified from the HPLC analysis of sonicated 4-CP whereas the intermediate peaks were not observed for the sonophotocatalytically treated 4-CP (Fig. 14). The enhanced sonophotocatalysis rate is due to the following reasons, the amount of production of effective free radicals gets increased when coupling the sonolysis and photocatalysis reactions. The enhanced mass transfer in the heterogeneous suspensions increases the efficacy. The catalysts may get excited to create the electronic charges by the application of visible light and ultrasound and the continuous cleaning of the surface of the catalysts by the ultrasound augments the mineralization process further.

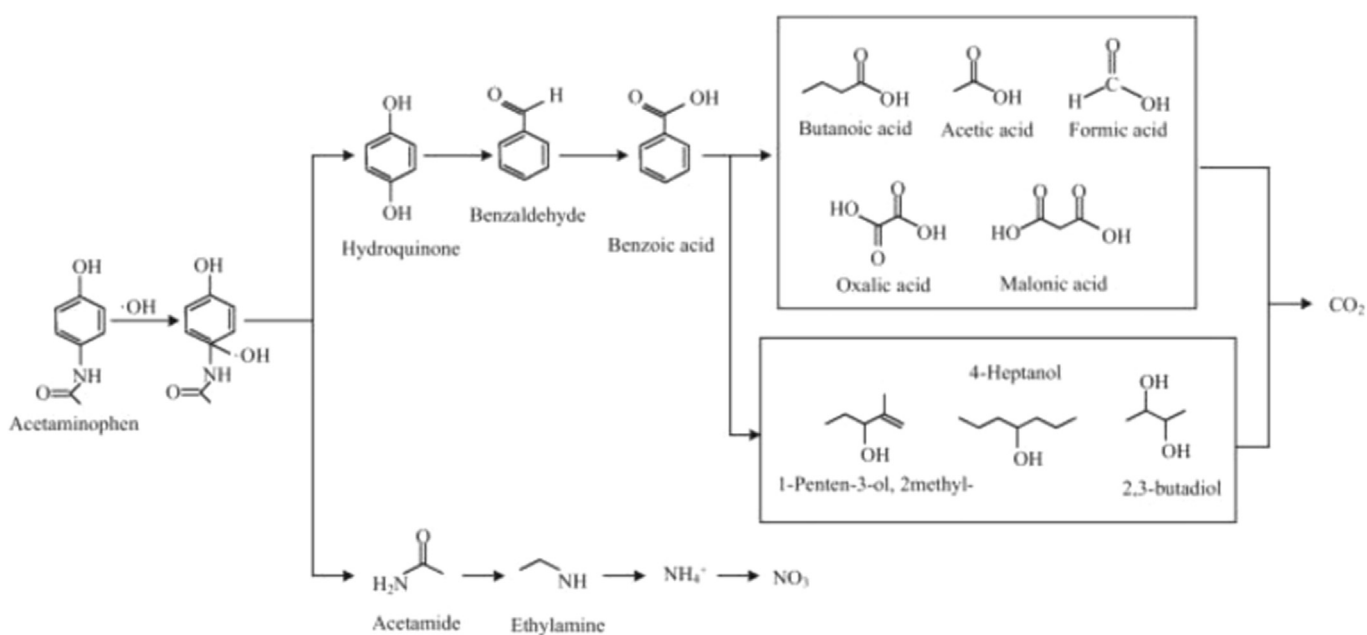
The proper mineralization is desirable before the disposal of the effluents to the environment to avoid the problems related with the discharge of organic contaminants. Saïen et al. [180] have examined the sonophotocatalytic degradation of copolymer, styrene-acrylic acid and investigated the influence of various parameters involved in the degradation process. Mrowetz et al. [181] have investigated the sonophotocatalytic degradation of Acid Red 1 and Acid Orange 8 in the presence of TiO<sub>2</sub> nanoparticles and observed the synergistic effect for the degradation of these azo dyes. Chen and Huang [182] sonophotocatalytically degraded nitrotoluenes and they found the various intermediates produced before its mineralization (Scheme 1). Safavi and Momeni [183] utilized the LC-MS technique to monitor the intermediates produced during the sonophotocatalytic degradation of various azo dyes. In addition, Madhavan et al. [67] have analyzed the various intermediates produced during the sonophotocatalytic degradation of an organophosphate insecticide. The major intermediates identified are dimethyl hydrogen phosphate, dimethyl phosphate, 3-hydroxybut-2-enamide and N-methyl-3-oxobutanamide during the degradation as presented in Table 3. The •OH radicals produced from the sonolysis of water are not producing any

hydroxylated derivatives since the insecticide is aliphatic in nature. Similar results were observed by Chen et al. [184] in the case of dimethyl methylphosphonate. The proposed mechanism for the degradation of dimethyl methylphosphonate was shown in Scheme 2 using the detected intermediates. The same set of intermediates are identified when performing the photocatalytic and sonophotocatalytic degradations which means ultrasound does not introduce principally different routes of dimethyl methylphosphonate degradation. The rate constants  $k_1$ – $k_7$  correspond to the conversion of one methoxy or methyl group at a time. The rate constant  $k_8$  denotes the conversion of dimethyl methylphosphonate into phosphoric acid without the formation of intermediates or else the conversion might have been completed before the identification of intermediates.

He et al. [175] have reported that mono-hydroxylated and demethylated methyl orange are the major intermediates found by the HPLC analysis (Fig. 15) during the sonophotocatalytic degradation of methyl orange in the presence of TiO<sub>2</sub>. The formation of demethylated methyl orange was not observed during the sonolysis whereas the intermediate was observed during the photocatalytic and sonophotocatalytic degradation of methyl orange. The proposed mechanism for the degradation of methyl orange has been shown in Scheme 3. The pH or the degradation process (sonolysis, photocatalysis, sonophotocatalysis) decides the yield and the production of by-products during the degradation of methyl orange. Similarly, Hapeshi et al. [185] have reported that approximately 20 intermediates were produced during the sonophotocatalytic degradation of ofloxacin which is the fluorinated quinolone type antibiotics. The various competing pathways for the degradation of ofloxacin have been shown in Scheme 4 in which piperazinyl dealkylation, hydroxylation, decarboxylation, defluorination, cleavage of ofloxacin and oxidation of hydroxyl groups are described as major transformation mechanisms. Most of the oxidation reactions have occurred in the N-piperazine ring whereas the main structure of ofloxacin was withstood. The identification of various intermediates produced during the degradation of various environmental pollutants is reported in the cited references for further studies [186–188]. The knowledge about the intermediates produced during the oxidation processes may help to understand the reaction pathway and mechanism of



**Scheme 7.** General reaction sequence proposed for the mineralization of picloram in aqueous acid medium by hydroxyl radicals following electro-Fenton process [222].



**Scheme 8.** Proposed acetaminophen degradation pathway [38].



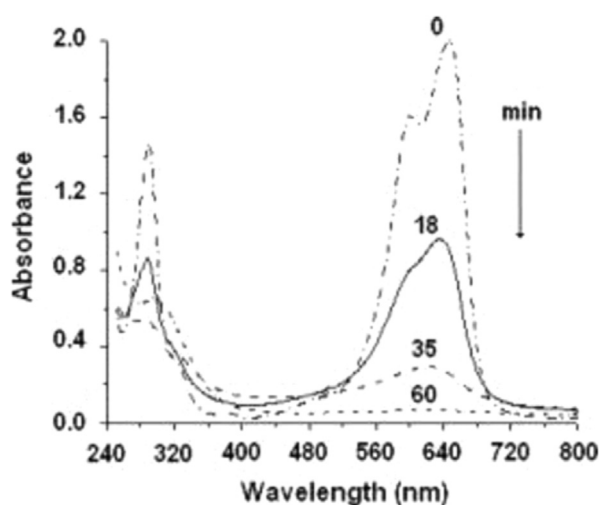


Fig. 19. Sono-electroFenton assisted degradation azure B [227].

the degradation. However more detailed studies in the form of controlled experimental conditions can help to find more number of intermediates or to synthesize the particular organic compound from oxidation processes [189,190].

The tentative mechanism of visible light assisted sonophotocatalytic degradation was reported by Riaz and Ashraf [191] and the schematic representation has been reproduced in Fig. 16. The ultrasonic irradiation reduces the recombination of electronic charges by disturbing the HOMO and LUMO positions of the semiconductor. The diffusion of electronic charges towards the bulk solutions was increased dramatically which leads to achieve the superior efficiency for the pollutant degradation. Meng et al. [173] have reported the mechanism for the sonocatalytic degradation of Rhodamine B in the presence CdS-C<sub>60</sub>/TiO<sub>2</sub> nanoparticles, the mechanism has been shown in Fig. 17. The major reason for the attained enhanced degradation of Rhodamine B is due to the production of improved number of non-selective radicals. The pathways for the production of free radicals are shown in Fig. 17. The band positions of TiO<sub>2</sub> and CdS are more suitable for the transformation of electronic charges and the ultrasonic irradiation produces light by the sonoluminescence process which further increases the direct band gap excitation of TiO<sub>2</sub>. The sonophotocatalytic degradation of various environmental pollutants such as perfluorooctanoic acid [192], phenols [193], chlorophenols [194], azo dyes [195–198], endocrine disruptors [199,200], agro-industrial effluents [201], herbicides [202], alkylbenzene sulfonate [203], 1,4-dioxane [204], 1,4-dichlorobenzene [205] are available in the literature for further studies. In addition to that, Anandan and Ashokkumar [206], He et al. [175,207], Singla et al. [208,209], Madhavan et al. [63–67], and Neppolian et al. [179] have utilized the wide range of ultrasound frequency for the sonophotocatalytic degradation of various environmental pollutants to show that the sonophotocatalytic degradation methodology is more suitable for the environmental remediation [210–213].

## 5. Combined sono, photo, electro, Fenton processes for the degradation of environmental pollutants

Hydrogen peroxide (H<sub>2</sub>O<sub>2</sub>) is decomposed under the catalysis of iron to generate the large number of hydroxyl radicals which completely degrade the various organic contaminants and this is called Fenton process. Generally, Fenton-based process suffers from narrow range of working pH and effective delivery of ferrous ions. To avoid the drawbacks associated with the Fenton process,

various Fenton like processes have been established and in situ generation of H<sub>2</sub>O<sub>2</sub> was developed to overcome the problems associated with the continuous generation of hydroxyl radicals [214,215]. The in situ generation of H<sub>2</sub>O<sub>2</sub> reveals the possibility of using other AOPs (photo, electro and ultrasound) along with the Fenton and Fenton like processes. The superior advantage of these combined methodologies is the regeneration of Fe<sup>2+</sup> from the oxidized iron ions. Therefore, combined sonoFenton, sonophoto-Fenton and sonoelectro-Fenton technologies are beneficial and avoid the drawbacks associated with Fenton systems. Mason and Petrier [216] and Petrier and Casadonte [217] have listed the degradation of various environmental pollutants by the sono-Fenton/photo-Fenton processes. The various automated processes involved in the photo-Fenton process [218] are shown in Scheme 5 for better understanding of the photo-Fenton assisted degradation of environmental pollutants.

Madhavan et al. [63,67] have obtained the enhanced mineralization of Acid Red 88 (AR88) and monocrotophos (MCP) during the sonophoto-Fenton assisted degradation. In the case of AR88, synergetic effect was observed after 2 h of irradiation whereas in the case of MCP, sonophotocatalysis with Fe<sup>3+</sup> occurs faster for the first two hours and then it tends to reach the same rate of removal with photocatalysis in the presence of Fe<sup>3+</sup> which may be due to the operation of coupled sonoFenton and photoFenton processes. Torres-Palma et al. [219] have reported the synergetic effect for bisphenol degradation during Fe<sup>2+</sup> ultrasound assisted photocatalytic degradation (Fig. 18). Bisphenol is one among the endocrine disrupting chemicals and produces the various intermediates during the degradation of various organic compounds. Therefore some additional attention must be paid to the intermediates produced during the degradation of phenols. Four or more steps are involved (Scheme 6) in the mineralization of bisphenol. The dissolved organic carbon (DOC) was taken into account to calculate the synergy (Eq. (3)) of the combined sonophotocatalytic and Fenton processes.

$$\text{Synergy} = \frac{\text{DOC}_{\text{combined}}}{\text{DOC}_{\text{ultrasound}} + \text{DOC}_{\text{photocatalysis}} + \text{DOC}_{\text{photo-fenton}}} \quad (3)$$

Ioan et al. [220] utilized the low ultrasonic frequency (45–47 kHz) to find out the efficiency of the sonoFenton process in degrading the bisphenol and found that the ultrasonic frequency is suitable for degradation. Chen et al. [221] demonstrated the Fenton-like process in the 40 kHz bath type ultrasonicator for the degradation of Orange II in the presence of 4A-zeolite supported  $\alpha$ -Fe<sub>2</sub>O<sub>3</sub> catalysts which are developed to enhance the in-situ generation of H<sub>2</sub>O<sub>2</sub>. The large surface area of 4A-zeolite produces an effective environment for the interaction of the pollutant and the hydroxyl radicals. Ying-Shih et al. [37] have reported the sonoFenton degradation of Carbofuran a well-known methylcarbamate pesticide which is used to inhibit insect activity. The addition of Fe<sup>2+</sup>/H<sub>2</sub>O<sub>2</sub> certainly enhanced the degradation of the target substance by effectively producing the hydroxyl radicals with the assistance of ultrasound.

In addition to these advanced oxidation processes, electro-Fenton process is a promising electrochemical treatment method for the degradation of wide variety of environmental contaminants [215]. Ozcan et al. [222] developed an electroFenton process for the complete mineralization of Picloram (4-amino-3,5,6-trichloro-2-pyridincarboxylic acid) which is a herbicide used for weed control. The proposed pathway for the complete mineralization of Picloram is shown in Scheme 7. Previously Ghauch [223], Rahman and Muneer [224] and Pavlovica [225] have attempted to mineralize the Picloram by using various AOPs and various intermediates have been observed instead of its complete mineralization. Chu et al. [226] have developed a dual cathode

**Table 4**  
Consecutive development of sonoelectrochemical studies [230].

Year	Event	Equipment/experimental condition	Important findings
1934	Water electrolysis under US influence	Platinum working electrode	Under US irradiation water electrolysis took place at lower voltages, electrolysis rate is faster than normal (silent) conditions
1957	Sonically assisted electroplating (nickel and chromium)	Frequencies of 10 and 260 kc/s	Same effects at both frequencies, depressed cathode polarization, slightly increased current efficiency, modified structural properties, decreased grain size, improved preferred orientation, improved hardness deposition, current densities over extended to higher values with the sound wave, decreased protection of porosity and corrosion, slightly improved adhesion and throwing power
1983	Diverse configurations and passivity of iron in sulfuric acid	Iron disks working electrode (diameter 3.8 cm, thickness of 0.16 cm) mounted on Plexiglas holder, 1.5 cm diameter exposed, 0.32 cm below plastic holder, wire soldered to disk's back for electrical contact, cell holder placed on rectangular Plexiglas tank of bottom area $15.2 \times 53.3 \text{ cm}^2$ , 17 cm deep electrolyte, 18 cm gauge platinum wire counter electrode, 25.4 cm long, ring shaped with 3.25 cm diameter, placed above iron disk, Hg/Hg <sub>2</sub> SO <sub>4</sub> reference electrode placed 0.5 cm from the working electrode, rubber mat leached in 2 N H <sub>2</sub> SO <sub>4</sub> on one end of the tank for good absorption, ultrasonic transducer co-axially gold-coated lead zirconate titanate ceramic spherical segment with a 5.08 cm diameter and 7.62 cm focal length, 1.58 MHz frequency	Curved piezoelectric transducer produced high frequency (1.58 MHz) US waves creating cavitation at the focal point, acoustic focal intensities generated up to $3.4 \text{ kW cm}^{-2}$ , low frequency (20 kHz) US produced using exponential microhorn, depassivation produced at high focal intensities (above $1.5 \text{ kW cm}^{-2}$ ) with single (100 ms) pulse US, low intensities require continuous US exposure, induced depassivation followed by precipitation of a metal salt film upon metal surface before the oxide film formation
1993	Electrode cleaning, effects of high-intensity ultrasound on glassy carbon Electrodes	Glassy carbon cylindrical electrodes, about 2 mm long, sealed in epoxy resin, conventional electrochemical cells, Pt auxiliary and Ag/AgCl (3M NaCl) reference electrodes, thermally jacketed by ethylene glycol coolant (12 °C), electrodes positioned parallel to the 1/2 in diameter Ti horn tip, placed in the center of the cavitation plume US processor, power output level of 10 (120- $\mu\text{m}$ peak tip amplitude), frequency 20 kHz, power 475 W, gap between Ti horn and glassy carbon electrodes 2 mm	Enhanced heterogeneous electron-transfer rates in dioxane, sonications in water gave no significant enhancement, surface roughness not changed appreciably after brief sonication in dioxane, except small amount of surface pitting, electrodes remained active for up to 5 days, prone to adsorb aromatic redox probes in aqueous media than polished electrodes, in water carbon surfaces are highly pitted, electroactive surface oxides density increased, kinetics improved after sonication in dioxane probably not associated with either increased microscopic electrode area or mediated electron transfer between surface oxides and solution analytes, but instead is likely to involve surface cleaning
1994	Voltammetry in the presence of US and surface effects	Three separate titanium tipped horn probes (13 mm diameter) extended by 127 mm, frequency 20 kHz, power up to $63 \text{ W cm}^{-2}$ , thermostatted EC cell with copper cooling coil inserted in the solution, water circulated from a constant-temperature bath (within 2 °C), platinum microdisk electrodes with radii between $2.5 (\pm 0.3)$ and $60.0 (\pm 5.0) \mu\text{m}$ , platinum macroelectrodes of radii between $0.05 (\pm 0.002)$ and $0.39 (\pm 0.01) \text{ cm}$ mounted on insulating Teflon sheath, polished using diamond lapping compounds to $0.25 \mu\text{m}$ , nickel electrode fabricated from a nickel wire with 1 mm diameter and 1.3 cm length utilized in Flade potential studies, electrode placed perpendicular to the axis of the horn at a distance of $30 (\pm 5) \text{ mm}$ , polished with diamond lapping compound to $0.25 \mu\text{m}$	Flade potential for the passivation of nickel in air-saturated aqueous KOH solution anodically shifted in the presence of US, voltammetric study of Cr(CO) <sub>6</sub> in acetonitrile solution feasible without the passivation observed under silent conditions where the electrolysis results in surface-active species, adsorption of species blocks further electron transfer
1995	Electrically separated EC cell and US bath	Voltammetry of potassium ferrocyanide: two compartment cell, platinum wire anode (1 cm $\times$ 0.3 mm), platinum foil counter electrode (2 cm <sup>2</sup> ), saturated calomel reference (SCE) electrode, scan rates either $50 \text{ mV s}^{-1}$ or $25 \text{ mV s}^{-1}$ , for low frequency of 25 kHz: $24 \text{ W cm}^{-2}$ fixed power output, liquid depth 15 cm, cell immersed, platinum electrode $\sim 3 \text{ cm}$ below liquid level; for high frequency bath of 800 kHz: power output variable approx. $18\text{--}61 \text{ W cm}^2$ , cell fitted closely into the focused resonant cavity with electrode 4 cm below liquid level, constant temperature of 5 °C	Simultaneous application of US to representative solution-phase, production of step-shaped voltammogram at platinum electrodes of both 'macro' and 'micro' dimensions in reversible voltammetric couples, increased limiting current with US power, least affected by US frequency (20–800 kHz region), complex voltammetry of a platinumized platinum electrode surface within the hydrogen adsorption regime in aqueous acid medium also least affected by sonication
	Penetration of sound waves in the glass wall of the EC reactor	Voltammetry of ferrocene: ultrasonic horn immersed in the solution (40 mm), electrode with radius $2.5 \mu\text{m}$ to 0.4 cm, three separate titanium tipped horn probes (diameter 13 mm) extended by 127 mm and operating at 20 kHz, power up to $63 \text{ W cm}^{-2}$ , thermostatted electrochemical with copper cooling coil inserted in the solution	
1996	Bipotentiostatic control, titanium tip for EC system	Dried and argon saturated electrolyte solutions, US generator made of titanium full wave probe (for media	Detection of one very broad reduction wave at more negative potential, may be due to a passive layer on

Table 4 (continued)

Year	Event	Equipment/experimental condition	Important findings
	US horn tip used as working electrode (sonotrode)	with low surface tension), 13 mm diameter, 20 kHz sound frequency, power of up to $80 \text{ W cm}^{-2}$ , thermostatted cell ( $25 \pm 2 \text{ }^\circ\text{C}$ ), Pt disk working electrode, 1 mm diameter, graphite rod counter electrode, saturated calomel reference electrode, titanium alloy immersion horn with tip placed opposite to a disk shaped working electrode which is oriented parallel (or perpendicular) to the vibrating horn tip, titanium horn electrically earthed Two sonotrode design: (1) titanium tip, 20 kHz sonic horn as working electrode, potentiostat mode connected through graphite rod touching the horn, (2) 0.15 cm Pt disk fitted into a tailored hole in the Ti tip using Araldite and insulated to act as an alternative working electrode, disk connected by wire through a hole drilled into the side of the tip, in both types of sonotrode the body of the horn insulated from the solution by means of a Teflon sheath and thermostatted the cell obtained using stainless steel cooling coil inserted in the solution, working electrodes (Ti horn tips or Pt disk inserts) polished using diamond lapping compounds to $0.25 \text{ }\mu\text{m}$ , three electrode potentiostat mode, carbon rod counter electrode, saturated calomel reference electrode, dried acetonitrile or water purified with resistivity $18 \text{ M}\Omega$ as background electrolyte	the titanium surface which allows only sluggish electron transfer, detection of extremely high limiting currents at sufficiently negative potentials with US  Untreated Ti alloy tip sonotrode gave behavior characteristic of the n-type semiconducting layer of $\text{TiO}_2$ , known to be present on the surface of metallic titanium, Platinum disk embedded in the titanium alloy tip of the horn probe gave high mass transport conditions and clean reversible electrochemistry for a variety of model systems
1997	Development of fundamental and applied aspects of US/EC	Baths and immersion horn probes as two major sources of US, piezo driven transducers limited to one frequency, often 20 kHz; three-electrode cell with an immersion horn incorporated in the center, well-thermostatted to within $\pm 2 \text{ }^\circ\text{C}$ , US horn immersed in solution and above working electrode, bipotentiostat with one working electrode connected to earth	Both physical and chemical processes involved, US affects through mass transport and thermal, use of multiphase systems and the detection of radical intermediates or real chemical effects of US remain largely unexplored, mixing or homogenization effect of power US drastically affects systems with more than one phase (gas–liquid, liquid–liquid or solid–liquid) and the rapid transport in the bulk phase due to turbulent convection, ideally suited for the development of the paired electrosynthesis, high energy liquid jets of some $100 \text{ ms}^{-1}$ impinging onto the electrode surface due to cavitation collapses near the electrode surface
1998	Mass transport enhancement by violent collapse of bubbles and shock waves in sonovoltammetry with hydrodynamic modulation from US  Diuron (herbicide) degradation using glassy carbon and BDD electrodes	Potentiostat mode, Pt disk working electrode (1.6 mm diameter), polished with diamond paste followed by alumina to $0.3 \text{ }\mu\text{m}$ , lead–zirconate–titanate (PZT) transducer driven, 20 kHz frequency, 475 W output power, PZT transducer coupled to titanium horn immersed in EC solution, standard macrotip ( $11 \times 13 \text{ mm}^2$ ) with maximum amplitude of $120 \text{ }\mu\text{m}$ , directly immersed sonicator horn with face immediately opposite and parallel to the working electrode surface, constant temperature of $22 \pm 1 \text{ }^\circ\text{C}$ , Ag/AgCl reference electrode for aqueous experiments, Ag/Ag for nonaqueous work, separated from the working electrolyte by a fine-porosity glass frit, Pt wire as auxiliary electrode, argon-saturated solutions to remove oxygen  Cyclic voltammetry and bulk electrolysis in 1:1 methanol:water solution with $\text{K}_2\text{SO}_4$ as supporting electrolyte, undivided cell in former case and H-type cell in the latter case with separate compartments using glass frits, potentiostat mode, glassy carbon disk anode (area $0.07 \text{ cm}^2$ ) for CV, glassy carbon plate ( $28 \times 13 \times 2 \text{ mm}^3$ ) in bulk electrolysis, silver wire and a platinum gauze as reference and counter electrodes, respectively, two sources of low-frequencies US, i.e. a cleaning bath with 35 kHz and 160 W, and a horn (area $1.0 \text{ cm}^2$ ) of titanium alloy with 20 kHz and power density $6 \text{ W cm}^{-2}$ , horn immersed in glass finger to attain electrical isolation from the solution, water flowing through this finger serves both as a cooling agent and as a coupling medium for transfer of US from the horn into the cell, finger with the horn immersed in anodic compartment (70 ml) of the H-type cell, 1–4 atm overpressured cooling water	Hydrodynamically modulated mass transport by US in EC due to combination of field-induced fluid motion driven at the frequency of the US and from the effects of acoustic cavitation observed in both aqueous and nonaqueous media, larger AC signal with increased cavitation activity, and a signal that is primarily driven at the US frequency results from field-induced motion occurred, current signal contains a time-independent DC component as well as a time-dependent AC component, DC signal arises from steady forces, primarily acoustic streaming, AC signal resulted due to combination of US field induced fluid motion and cavitation effects, DC component assumed to result from acoustic streaming but may be affected by the intensity of cavitation Major oxidation isolated with 23% yield from the loss of one electron and one proton with formation of a nitrogen radical and of the corresponding N–N dimer, two more compounds isolated with 12% and 10% yields suggested to originate from an intramolecular Fries rearrangement, i.e. migration of an amide group from a monomeric unit of the dimer to the aromatic ring of the second one, with formation of a dichloro-N, N-dimethyl benzamide derivative, several non-identified minor compounds also generated which could involve multi-electron oxidation processes since the overall oxidation process of diuron required more than one electron
1999	Tungsten-supported boron-doped CVD diamond electrodes under US/EC	Cylindrical tungsten substrates (5 mm diameter, 5 mm height), BDD electrodes mounted on Teflon holders by heat-shrink procedure, electrical connection by spot-welding a nickel contact to the reverse side of the	Highly boron-doped (atomic concentration $1020\text{--}1021 \text{ cm}^{-3}$ ) conductive diamond films deposited on tungsten substrates by hot-filament assisted chemical vapor deposition from a gaseous feed of methane and

Table 4 (continued)

Year	Event	Equipment/experimental condition	Important findings
		tungsten substrate, potentiostat mode, thick gold wire counter electrode, saturated calomel reference electrode, argon degassed solution, mixture of KCl, orthophosphoric acid, NaOH and ultrahigh quality water of a resistivity not less than 18 MΩ cm as electrolyte, 20 ± 2 °C constant temperature	diborane in hydrogen, standard rate constant for electron transfer is $3 \times 10^{-3} \text{ cm s}^{-1}$ , EC processes at 90 W cm <sup>-2</sup> , sonication without significant electrode deterioration, surface property changed due to anodic polarization, increased current after negative polarization, voltammograms under US conditions suggested potential pretreatment with possible process switching from nearly mass-transport controlled to virtually absent mass transport
2001	Depassivation of electrode by ultrasound	250 cm <sup>3</sup> working volume cell, 25 ± 2 °C constant temperature, BDD anode (5 × 5 mm <sup>3</sup> ), mounted on Teflon, coiled platinum wire counter electrode, saturated calomel reference electrode, electrical connection to the rear (graphite) side via a brass rod attached using silver epoxy resin, the rear of electrode assembly enclosed using a sealant-wax, whole unit placed near the bottom of the cell, directly opposite from 13 mm diameter titanium tip of a US horn, frequency 20 kHz, US intensity 14 W cm <sup>-2</sup> , elimination of bipotentiometric control of titanium horn by insulating the transducer from probe with Teflon disk, 10 mm gap between transducer probe and working electrode	US assisted cathodic stripping voltammetry at BDD electrode for detection of lead, concentrations above 3 mM, linear sweep voltammetry gave analytical signal from a cathodic strip of electrodeposited PbO <sub>2</sub> , linearity observed from 3 ± 100 mM, lower detection limit 3 mM, square-wave voltammetry to lower the detection limits with linearity of the order of 10 <sup>-8</sup> M
2001	Heavy metal determination analysis	Working electrode face on to US horn with a gap of 5 mm, horn equipped with a titanium alloy microtip (diameter 3 mm), 20 kHz frequency, power intensity 200 ± 5 W cm <sup>-2</sup> , thermostatted with stainless steel cooling coil inserted, temperature 25 ± 3 °C, bipotentiometric control of the titanium horn by insulating the transducer from the probe with a thin Teflon disk and connecting with a screw, 3 mm diameter glassy carbon disk electrode plated in situ with mercury from a 1 mM solution, polished using diamond lapping compounds to 0.1 mm, saturated calomel reference electrode, 20 cm coiled platinum wire counter electrode	Enhanced mass transport to the electrode surface and cavitation depassivation maintaining surface activation during preconcentration, good intrasample reproducibility and favorable with independent analysis of the mucous extract by electro-thermal atomic absorption spectroscopy, theoretical detection limit of 0.004 ppm determined, sonoelectroanalysis facilitates the use of a nondestructive biomarker for the detection of heavy metals with the following advantages: minimal experimental procedure, elimination of sample pretreatment, possibility for portable apparatus and relatively inexpensive compared with either ICPAES or AAS giving it the potential to become a powerful and useful field apparatus
	Reactive dye Procion Blue degradation	250 ml cell, BDD films deposited tungsten wires as working electrode (1 mm diameter, 10 mm length), platinum counter electrode, saturated calomel reference electrode, working electrode fitted into Teflon holder and placed at the cell's bottom, frequency 24 Hz, power 200 W, maximum intensity 30 W cm <sup>-2</sup> , 13-mm-diameter glass horn, phosphate buffer solutions prepared from deionized water (resistivity 18 MΩ cm), degassed with argon	Direct partial oxidation with four electron transfer under solvent window up to 2.5 V vs. SCE in PBS (pH 2), extensive degradation of Procion Blue does not occur at potentials below the required one for solvent decomposition, oxidation most easily achieved in acidic solution and at low dye concentrations, electrode surface fouling noted under alkaline pH and at higher dye concentrations, influence redox processes which are directly associated with defect sites on the diamond electrode itself
2003	N,N-dimethyl-p-nitrosoaniline degradation	Conventional three-electrode arrangement, potentiostat mode, free-standing 2 mm × 5 mm polycrystalline BDD electrodes rich in graphitic impurity states and grown in house on tungsten rod substrates (1 mm diameter, 10 mm length) as working electrode, platinum coil counter electrode, saturated calomel reference electrode, frequency 24 kHz, output power approximately 8 W cm <sup>-2</sup> , 13 mm diameter glass horn	US power drastically improves bleaching rate by increasing the rate of mass transport at the electrode-solution interface, initially more efficient bleaching process using BDD electrodes rich in sp <sup>2</sup> carbon impurity states, appearance of reactive intermediates such as hydroxyl radicals preferentially in the vicinity of impurity states, mass transport dominated in controlling the efficiency of bleaching process
2007	Sonovoltammetric determination of 4-nitrophenol on diamond electrodes	Three electrode arrangement with one-compartment Pyrex glass cell (50 mL), N <sub>2</sub> degassing, BDD films with 8000 ppm boron content as working electrode, exposed area 0.25 cm <sup>2</sup> , Ag/AgCl (3.0 mol L <sup>-1</sup> KCl) reference electrode, 1 cm <sup>2</sup> Pt foil counter electrode, US horn tip placed in front of working electrode, computer controlled potentiostat, bipotentiostatic control of the titanium horn tip with insulated transducer from the probe using Teflon disk, 20 kHz frequency, 20% and 40% power intensity, amplitude 20%, acoustic power 14 W, acoustic energy transferred 155 and 178 J for oxidation and reduction processes of 4-nitrophenol on the diamond electrode, respectively, supporting electrolyte is Britton-Robinson 0.1 mol L <sup>-1</sup> , pH 6.0 adjusted using NaOH 1.0 mol L <sup>-1</sup>	Significant improvements in the analytical sensibility observed due to electrode surface cleaning and the enhancement in the transport of species to the electrode surface provided by US, limit of detection for oxidation and reduction processes diminished from 11.7 to 3.87 and from 6.38 to 2.57 μg L <sup>-1</sup> , respectively
2008	Phenols degradation	Cylindrical single-compartment cell, BDD or Pt anode with 24 cm <sup>2</sup> immersed area as working electrode, titanium foil with same area as cathode, interelectrode gap 1 cm, current density 20 mA cm <sup>2</sup> , pH 3.0 adjusted with 0.2 M H <sub>2</sub> SO <sub>4</sub> , 200 cm <sup>3</sup> phenol sample volume, 10 °C constant temperature, solution volume 200 cm <sup>3</sup> , frequency 33 kHz, power 50 W	With US, for BDD, increased degradation rate and current efficiency are 301% and 100%, respectively, for Pt 51% and 49%, respectively, increased diffusion coefficient for BDD and Pt are 375% and 42%, respectively, US effect on BDD much greater than for Pt, without US large adsorption of phenol on both electrodes, with US, the adsorption amount

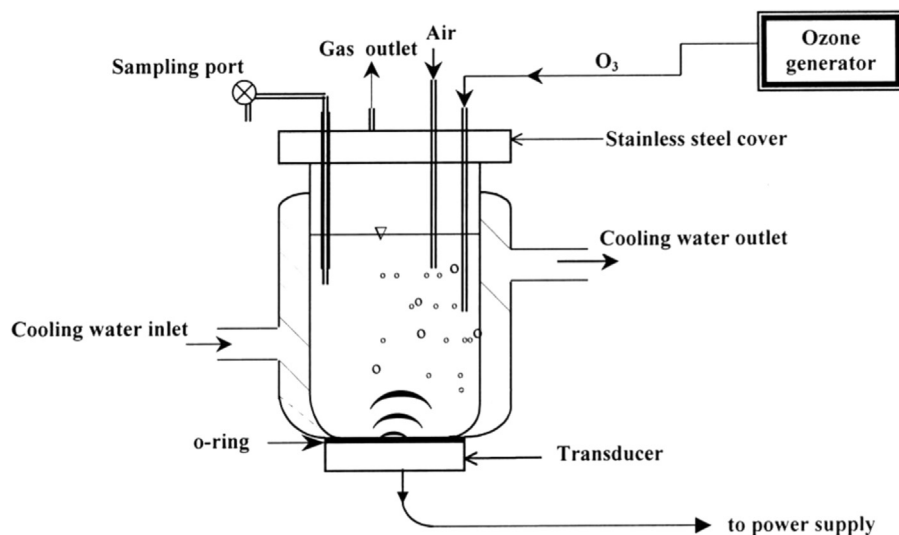
Table 4 (continued)

Year	Event	Equipment/experimental condition	Important findings
2009	Methylparathion determination in potato and corn extracts 4-Nitrophenol degradation in lemon and orange juices	50 mL one compartment pyrex glass cell with three electrode arrangement, N <sub>2</sub> degassing, BDD films with 8000 ppm boron content working electrode (0.25 cm <sup>2</sup> area), Ag/AgCl (3.0 mol <sup>-1</sup> KCl) reference electrode, 1 cm <sup>2</sup> Pt foil counter electrode, US horn tip placed in front of working electrode face (gap 5 mm), computer-controlled potentiostat mode, bipotentiostatic control of titanium horn tip, insulated transducer from the probe with Teflon disk, Britton-Robinson (BR) 0.1 mol L <sup>-1</sup> buffer optimized at pH 7.0 for methylparathion and at pH 6.0 for 4-nitrophenol as supporting electrolyte. 20% US intensity, 14 W power, 20 kHz frequency	decreased by 79% and 56% on BDD and Pt electrodes, respectively, renewal and activation effect of US on the surface of BDD more obvious than Pt, enhancement for EC by US on BDD is 108% and for Pt is only 25%, degradation of phenol on BDD easier than Pt, lower amount of intermediates produced at BDD than Pt Detection limit for methylparathion in water and corn extract were 4.86 and 10.1 µg L <sup>-1</sup> , respectively, 55% and 72% lower than silent voltammetry, 83.5% and 96.2% recovery values, possible reasons are electrode surface cleaning and mass transport enhancement toward the electrode surface
2010	Voltammetric scale up to pre-pilot stage using trichloroacetic acid (TCAA)  Substituted phenols degradation at low-frequency (40 kHz)	Laboratory glass sonochemical reactor (adapted as sonoelectrochemical device) used for bulk electrolysis in batch mode, galvanostat (120 mA, 13.4 V maxima power), catholyte volume 200 mL, for divided mode, a Nafion 450 cationic membrane to separate catholyte and anolyte chambers, with anolyte volume 200 mL, for non-optimized flow-sonoelectrochemical system used for the scale-up of the process, polypropylene reactor designed for divided and undivided configuration, catholyte and anolyte volume 2000 and 1000 mL, respectively, titanium disk with $d=4$ mm, 0.126 cm <sup>2</sup> and spiral wound platinum wire cathode for voltammetric experiments, for bulk electrolyses, mesh-plate of Ti with 2 cm <sup>2</sup> of active area in each electrode face in the batch cell and 20.0 cm <sup>2</sup> in the flow cell used as cathodic material and platinized titanium (Pt/Ti) mesh with 20 cm <sup>2</sup> as anodic material in both scales, reference electrode is an Ag/AgCl/KCl (3 M), supporting electrolyte Na <sub>2</sub> SO <sub>4</sub> purged with argon to avoid oxygen entrance, frequency 358,850,863 kHz, power 0.039, 0.047, 0.054 W Constant current density (20 mA cm <sup>-2</sup> ), room temperature (25 °C), 250 mL electrolyte (1 mM substrate + 0.2 M Na <sub>2</sub> SO <sub>4</sub> ), magnetically stirring for EC, frequency 40 kHz, power 150 W, BDD or PbO <sub>2</sub> anode with 4 cm <sup>2</sup> geometric area, same sized stainless steel sheet cathode, electrode gap 10 mm	US alone gave poor performance compared to US/EC, batch scale US/EC analyses with horn-transducer 24 kHz positioned at about 3 cm from the electrode surface achieved little degradation, but specifically designed US/EC reactor (not optimized) during the scale-up provided better results (fractional conversion 97%, degradation efficiency 26%, selectivity 0.92 and current efficiency 8%) at lower ultrasonic intensities and volumetric flow  Enhancement more obvious at BDD anodes than at PbO <sub>2</sub> anodes, at BDD anode, 73–83% disappearance of p-substituted phenol and 60–70% for COD removal, for PbO <sub>2</sub> anode, 50–70% disappearance of p-substituted phenols and only 5–25% for COD removal, different enhancement extent due to diverse effects of ultrasound on specialized types of hydroxyl radicals, hydroxyl radicals free at the BDD electrodes with a larger reaction zone whereas adsorbed at the PbO <sub>2</sub> electrodes with a smaller reaction zone
2011	Un-hydrolyzed/hydrolyzed reactive blue (RB) 19 dye degradation	Perspex sheet undivided electrolytic cell, lead oxide working electrode (14 × 15 cm <sup>2</sup> ), stainless mesh steel counter electrode, working and counter electrode positioned vertically and parallel to each other with gap 2.5 cm, DC power supply, Digital Ultrasonic Bath, frequencies 20–80 kHz, pH 3–9 controlled using 1 M NaOH or 1 M HCl	90% color removal, 56% TOC removal at frequency 80 kHz, pH 8 after 120 min, un-hydrolyzed RB 19 dye formed acetic acid, benzoic acid etc. after 30 minutes with the complete removal of dye, for hydrolyzed dye, 10 min was enough, first order kinetics, US/EC better than individual processes, total energy consumption reduced to half
Present	General US/EC, US/EC-oxidation, optimization, organic synthesis	–	–

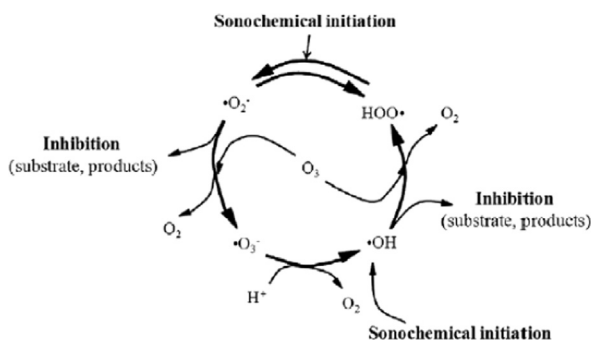
oxidation system for the enhanced electro-Fenton assisted mineralization of 4-nitrophenol. Luna et al. [38] have investigated the electro-Fenton assisted mineralization of acetaminophen (also called Paracetamol) which is one among the most frequently used drugs worldwide. The proposed pathway for the electro-Fenton assisted mineralization of Paracetamol is shown in Scheme 8.

In order to further enhance the efficiency of removing the environmental contaminants by the electro-Fenton process, it is coupled with ultrasound and/or photoirradiation source to produce the novel hybrid technologies. Martinez et al. [227] have reported the sonoelectro-Fenton assisted degradation of azure B as represented in

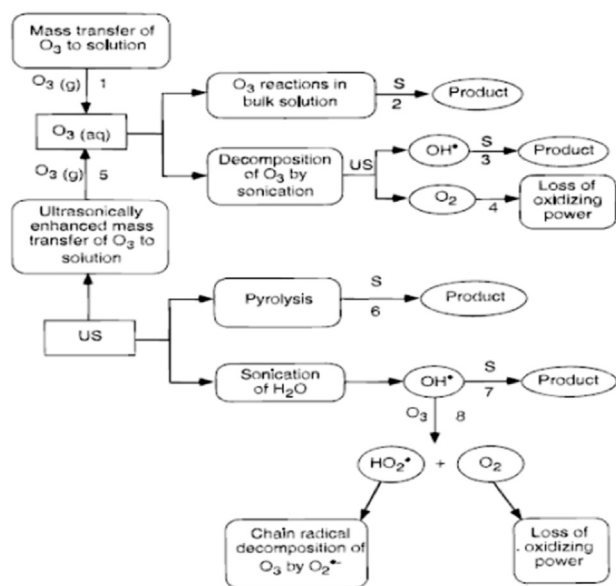
Fig. 19. The efficiency of degradation of azure B is of the following order: sonoelectro-Fenton > Fenton > sonolysis. The suitable reason for the observed synergetic effect in the degradation of azure B is due to the electrocatalytic in situ generation of H<sub>2</sub>O<sub>2</sub> followed by the formation of various number of free radicals [227]. In addition to that, Zhong et al. [228] and Cong et al. [229] have reported the heterogeneous sonophoto-Fenton and photoelectro-Fenton assisted degradation of Acid Orange 7 and phenol. Similar kind of methodologies have been developed by researchers and they have achieved the enhanced efficacy of removal of various environmental pollutants. The degradation of numerous environmental pollutants by Fenton,



Scheme 9. Schematic diagram of the experimental setup [20].



Scheme 10. Initiation, promotion, and inhibition of the decomposition of  $O_3(aq)$  under ultrasonic irradiation [36].



Scheme 11. Conceptual diagram of possible pathways of substrate (S) degradation and interactions of sonolysis and ozonolysis [233].

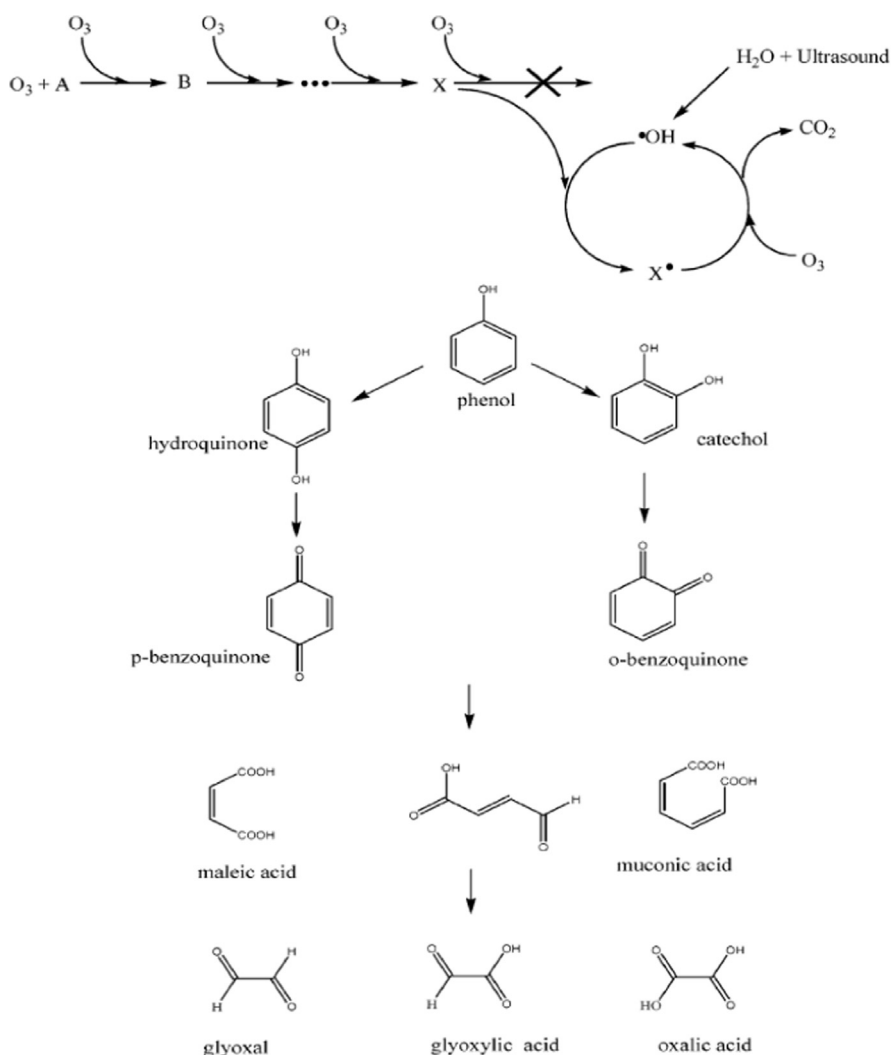
photoFenton, electroFenton, photo-electronFenton, sonoFenton, sonophoto-Fenton and sonoelectro-Fenton technologies have showed the alternative growing methodologies for the cost effective

degradation of environmental pollutants and much of the early work of Fenton process has been reported elsewhere [214,215]. The sequential growth of the sonoelectrochemical degradation of various environmental pollutants has been reported by Thokchom et al. [230] which is reproduced in Table 4 to understand how the growth of sonoelectrochemical technologies is utilized for the pollutants degradation.

## 6. Combined sonolysis with ozonolysis process for the degradation of environmental pollutants

Ozonolysis is another type of AOP which accounts for the production of numerous radicals during the oxidation of contaminants by ozone (Table 1). Ozonolysis reactions have been carried out by the following different combinations in order to enhance the degradation,  $O_3$ ,  $US/O_3$ ,  $O_3/H_2O_2$ ,  $O_3/UV$ ,  $O_3/UV/H_2O_2$ /  $US$ ,  $O_3/UV/H_2O_2$  and heterogeneous catalytic ozonation. Among the various AOPs, sonolysis combined with ozonolysis gave the synergetic effect for the degradation of environmental pollutants [231]. There are numerous opportunities available to study the degradation of environmental pollutants by the hybrid ultrasound assisted ozonolysis. Nevertheless there are few reports available in the literature to explain the fundamental processes and these reports demonstrate the effect of degradation of environmental pollutants by the combined ozonolysis with sonochemistry [36,231–236]. A model reactor setup is shown in Scheme 9 as reported by Ince and Tezcanli [20] to carry out the combined ozonolysis and sonochemical degradation. The initiation, promotion, and inhibition of the decomposition of  $O_3(aq)$  under ultrasonic irradiation has been schematically (Scheme 10) reported by Destailats et al. [36] which gives a clear idea about the various pathways involved in the combined system. Alternatively, Weavers et al. [233] have reported the various possibilities for the decomposition of ozone in the presence of ultrasound as represented in Scheme 11. The various pathways involved in the schematic diagram have been discussed elsewhere [36,233]. The ultrasound assisted decomposition of  $O_3$  enhances the production of  $\bullet OH$  radicals. The synergetic effect has been achieved for the degradation of Azobenzene and Methyl Orange by the combination of these two AOPs [36].

Lesko et al. [231] have reported the various pathways involved in the degradation of phenol by the combined ultrasound and ozonation as represented in Scheme 12. The reason for the



**Scheme 12.** Proposed reaction mechanism for the oxidation of phenol with ultrasonic irradiation combined with ozonolysis resulting the total elimination of TOC [231].

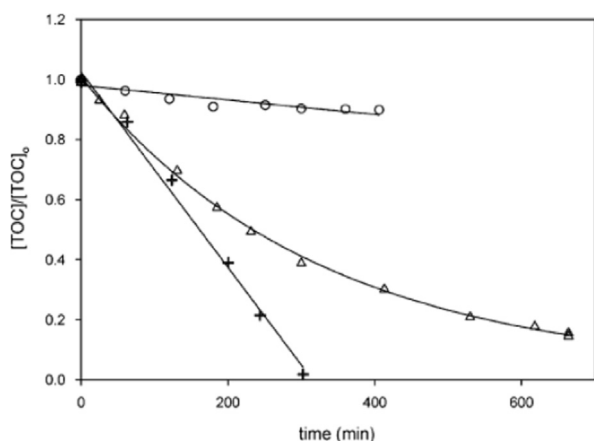


**Fig. 20.** TOC loss during phenol oxidation by ultrasound assisted ozonolysis [231].

observed synergetic effect may be due to the decomposition of  $O_3$  by  $\bullet OH$  radicals produced from the sonolysis which initiate the chain type free radical reaction for the degradation of organic contaminants. The complete mineralization of phenol (Fig. 20) was achieved within 5 h which has given the proficiency of the combination of these AOPs. Muthukumar and Selvakumar [237] have reported that the  $\bullet OH$  radicals have the highest oxidation potential of 2.8 V and easily decompose the ozone molecules to produce the

various number of non-selective free radicals which enhance the degradation of environmental pollutants. Similarly, Gogate and Pandit [238] have observed the synergetic effect during the phenol degradation by the combination of sonolysis with ozonation and proposed that the reason for the observed synergetic effect is only due to the attack of free radicals with the target substances and the enhanced production of these free radicals controlling the mechanism of the degradation. In the case of colored pollutants, the ozone molecules rapidly and selectively attack the unsaturated bonds of the effluents resulting in the rapid removal of color [25,28]. However, ozonation combined with sonolysis enhanced the mineralization of Direct Red 23 as reported by Song et al. [239] and the various pathways involved in the mineralization process are shown in Scheme 13. Both sonolysis and ozonation are known to produce  $\bullet OH$  radicals in aqueous solutions, which may attack the Direct Red 23, thus beginning the degradation; naphthalene-2-sulfonic acid, 1-naphthol, urea and acetamide have been identified as the major intermediates by gas chromatography coupled with mass spectrometry technique. Further treatment of the intermediates with the combined AOPs tends to completely mineralize the pollutants.

Heterogeneous ozonation is also another important AOP for improving the proficiency of degradation of various intermediates produced during the ozonolysis [240]. The combination of ozonolysis in the presence of nanocatalysts can provide the effective environment for the interaction of various free radicals with the





the sonocatalytic ozonation technique to mineralize the diclofenac. The mineralization mechanism is shown in Scheme 14 in order to understand the various intermediates produced during the diclofenac degradation. The mechanism of diclofenac mineralization was categorized as I–V, I indicates the parent compound,

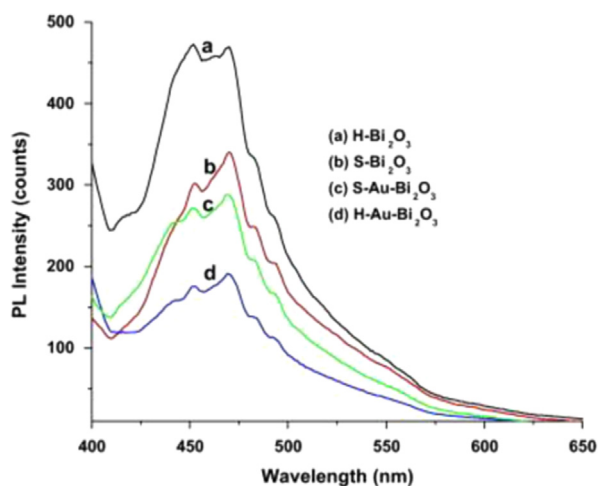
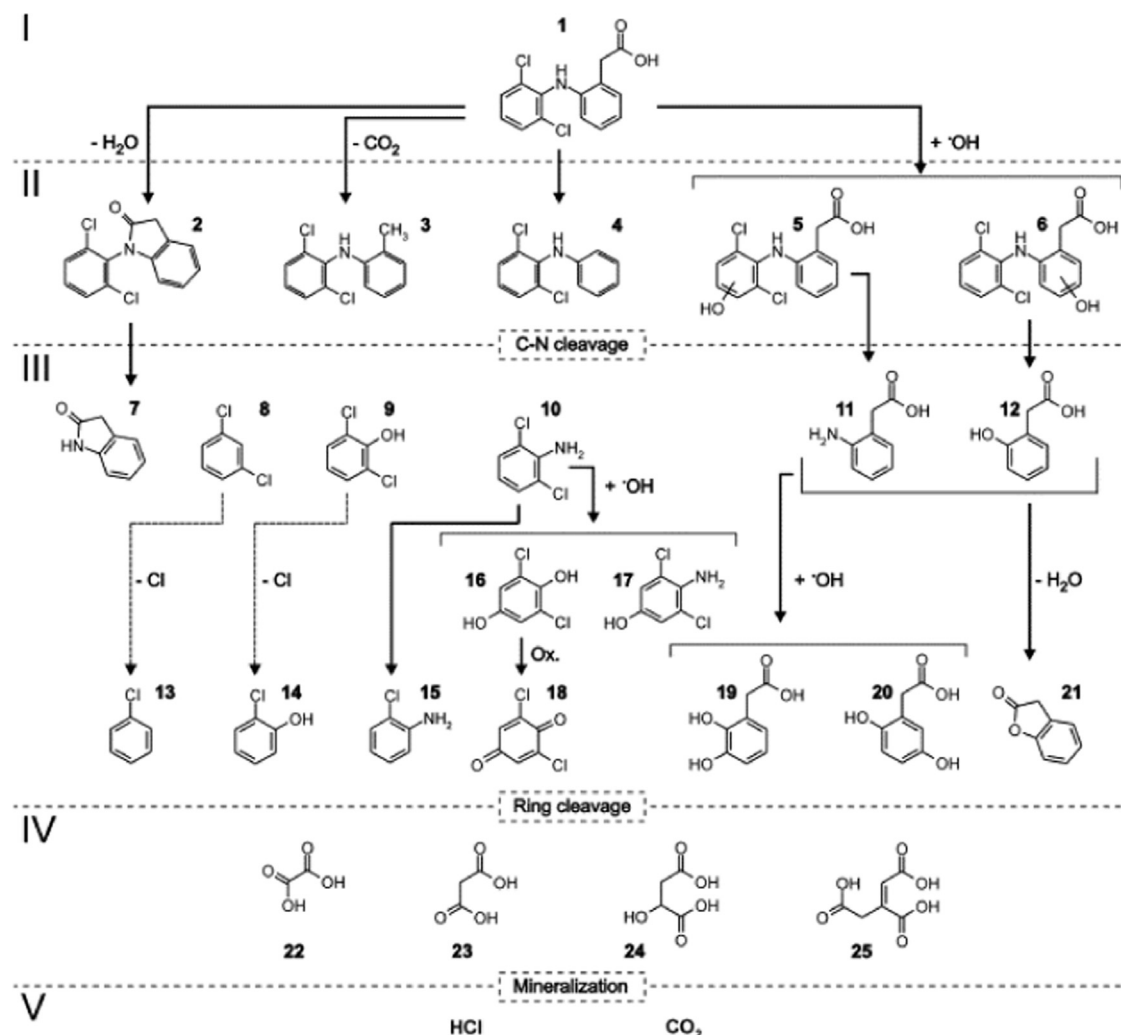


Fig. 21. Photoluminescence spectra (excited at 367 nm) of various nanocatalysts [141].

II–IV are the various intermediates produced during the mineralization and V informs the complete mineralization of diclofenac. Much of the early work of ozonolysis and sonolysis has been reviewed elsewhere [241,242] for future studies. However, development of coupled AOPs such as sonophotocatalysis with ozonolysis and ozonation coupled with sonophoto-Fenton, sonoelectro-Fenton and sonoelectrophoto-Fenton and novel hybrid technologies can enhance the mineralization of wide spectrum environmental contaminants within a short time duration.

## 7. Conclusions

In this review, the various advanced oxidation processes have been summarized for the degradation of recalcitrant organic contaminants. AOPs are the most studied technologies for the degradation of various environmental contaminants among the numerous technologies reported so far. The various treatment methodologies discussed in this review have their own advantages and disadvantages for the environmental purification. Nevertheless the efficiency of an AOP can be premeditated based on the production of effective radicals in addition to the pollutants characteristics like pH, concentration of contaminants, salinity and features of the intermediates. The ultrasonic irradiation (sonolysis) alone is ineffective for the degradation of various environmental contaminants particularly for the hydrophilic contaminants.



Scheme 14. Proposed degradation scheme in the sonolysis of diclofenac in water (617 kHz, 90 W) [35].

However, the maximum efficiency of degradation of environmental pollutants can be harvested by the combination of various AOPs. The combination of ultrasound with other AOPs certainly enhances the production of powerful non-selective radicals which improves the degradation process and avoids the secondary pollution. The combinations of ultrasound with other AOPs are economically more attractive when compared with the application of AOP techniques alone for the environmental purification.

The challenges associated with the development of combined AOPs are to be solved in the near future by reducing the cost consumption phenomena. The development of suitable reactor setup for the sonolytic reactions reduces the electrical consumption considerably. The utilization of solar (visible) light instead of ultra-violet source for photoexcitation of the semiconductor materials is another important aspect to be developed to reduce the cost of the hybrid technologies further. In addition to that, development of methodologies to overcome the drawback of the Fenton reactions and ozonolysis process can further enhance the efficiency of the combined AOPs and significantly reduce the cost consumption of the contaminants treatment processes. The wastewater treatment by the ultrasound assisted techniques can enhance the quality of the water which can be used for the domestic and irrigation purposes.

## Acknowledgments

The authors would like to thank FONDECYT Postdoctorado project No.: 3120095 and FONDECYT No.: 1130916, Government of Chile, Santiago, for financial assistance.

## References

- Olsson G. Water and energy: conflicts and connections. *Water* 2012;21:12–4.
- Eikebrokk B, Vogt RD, Liltved H. NOM increase in Northern European source waters: discussion of possible causes and impacts on coagulation/contact filtration processes. *Water Sci Technol: Water Supply* 2004(4):47–54.
- Korth A, Fiebiger C, Bornmann K, Schmidt W. NOM increase in drinking water reservoirs – relevance for drinking water production. *Water Sci Technol: Water Supply* 2004(4):55–60.
- Ustun AP, Corvalan C. Preventing disease through healthy environments: towards an estimate of the environmental burden of disease. Geneva, Switzerland: WHO Publishers; 2006. p. 1–104.
- Batterman S, Eisenberg J, Hardin R, Kruk ME, Lemos MC, Michalak AM, et al. Sustainable control of water-related infectious diseases: a review and proposal for interdisciplinary health-based systems research. *Environ Health Perspect* 2009;117:1023–32.
- Adewuyi YG. Sonochemistry: environmental science and engineering applications. *Ind Eng Chem Res* 2001;40:4681–715.
- Devipriya S, Yesodharan S. Photocatalytic degradation of pesticide contaminants in water. *Sol Energy Mater Sol Cells* 2005;86:309–48.
- Preziosi P. Natural and anthropogenic environmental oestrogens: the scientific basis for risk assessment. *Endocrine disruptors as environmental signalers: an introduction*. *Pure Appl Chem* 1998;70:1617–31.
- Tyler CR, Routledge EJ. Oestrogenic effects in fish in English rivers with evidence of their causation. *Pure Appl Chem* 1998;70:1795–804.
- Muller S, Schlatter C. Estrogenic potency of nonylphenol in vivo – a case study to evaluate the relevance of human non-occupational expo-sure. *Pure Appl Chem* 1998;70:1847–53.
- Dejohn PB, Hutchins RA. Treatment of dye wastewaters with granular activated carbon. *Text Chem Color* 1976;8:34–8.
- Patil SS, Shinde VM. Biodegradation studies of aniline and nitrobenzene in aniline plant wastewater by gas chromatography. *Environ Sci Technol* 1988;22:1160–5.
- More AT, Vira A, Fogel S. Biodegradation of trans-1,2-dichloroethylene by methane-utilizing bacteria in an aquifer simulator. *Environ Sci Technol* 1989;23:403–6.
- Fujishima A, Honda K. Electrochemical photolysis of water at a semiconductor electrode. *Nature* 1972;238:37–8.
- Slokar YM, Marechal AML. Methods of decoloration of textile wastewaters. *Dyes Pigm* 1998;37:335–56.
- Venkatahari R, Peters RW. Chemical oxidation technologies: ultraviolet light/hydrogen peroxide, Fenton's reagent, and titanium dioxide-assisted photocatalysis. *Hazard Waste Hazard Mater* 1993;10:107–49.
- Jain VK. Supercritical fluids tackle hazardous wastes. *Environ Sci Technol* 1993;27:806–8.
- Scott JP, Ollis DF. Integration of chemical and biological processes for water treatment: Review and recommendations. *Environ Prog* 1995;14:88–103.
- Joseph CG, Puma GL, Bono A, Krishnaiah D. Sonophotocatalysis in advanced oxidation process: a short review. *Ultrason Sonochem* 2009;16:583–9.
- Ince NH, Tezcanli G. Reactive dyestuff degradation by combined sonolysis and ozonation. *Dyes Pigm* 2001;49:145–53.
- Ollis DF, Al-Ekabi H. Photocatalytic purification and treatment of water and air. Amsterdam: Elsevier; 1993.
- Serpone N, Pelizzetti E. Photocatalysis, fundamentals and applications. New York: Wiley; 1989.
- Schiavello M. Photocatalysis and environment. Dordrecht: Kluwer; 1988.
- Hordern BK, Ziolk M, Nawrocki J. Catalytic ozonation and methods of enhancing molecular ozone reactions in water treatment. *Appl Catal B: Environ* 2003;46:639–69.
- Salome O, Soares GP, Orfao JM, Portela D, Vieira A, Fernando M, et al. Ozonation of textile effluents and dye solutions under continuous operation: Influence of operating parameters. *J Hazard Mater* 2006;137:1664–73.
- Hassan MM, Hawkyard CJ, Barratt PA. Decolourisation of dyes and dyehouse effluent in a bubble-column reactor by ozonation in the presence of H<sub>2</sub>O<sub>2</sub>, KMnO<sub>4</sub> or ferral. *J Chem Technol Biotechnol* 2006;81:158–66.
- Surpateanu M, Zaharia C. Advanced oxidation processes for decolorization of aqueous solution containing Acid Red G azo dye. *Cent Eur J Chem* 2004;2:573–88.
- Acar E, Ozelge T. Oxidation of Acid Red-151 aqueous solutions by the peroxone process and its kinetic evaluation. *Ozone Sci Eng* 2006;28:155–64.
- Zhao L, Sun Z, Ma J. Novel relationship between hydroxyl radical initiation and surface group of ceramic honeycomb supported metals for the catalytic ozonation of nitrobenzene in aqueous solution. *Environ Sci Technol* 2009;43:4157–63.
- Beltran FJ, Rivas FJ, Fernandez LA, Alvarez PM, Montero-de-Espinosa R. Kinetics of catalytic ozonation of oxalic acid in water with activated carbon. *Ind Eng Chem Res* 2002;41:6510–7.
- Beltran FJ, Rivas FJ, Montero-de-Espinosa R. Ozone-enhanced oxidation of oxalic acid in water with cobalt catalysts. 2. Heterogeneous catalytic ozonation. *Ind Eng Chem Res* 2003;42:3218–24.
- Madhavan J, Sathishkumar P, Anandan S, Zhou M, Grieser F, Ashokkumar M. Ultrasound assisted photocatalytic degradation of diclofenac in an aqueous environment. *Chemosphere* 2010;80:747–52.
- Suslick KS, Hammerton DA, Cline RE. Sonochemical hot spot. *J Am Chem Soc* 1986;108:5641–2.
- Anandan S, Lee G, Chen P, Fan C, Wu JJ. Removal of orange II dye in water by visible light assisted photocatalytic ozonation using Bi<sub>2</sub>O<sub>3</sub> and Au/Bi<sub>2</sub>O<sub>3</sub> nanorods. *Ind Eng Chem Res* 2010;49:9729–37.
- Hartmann J, Bartels P, Mau U, Witter M, Timpling WV, Hofmann J, et al. Degradation of the drug diclofenac in water by sonolysis in presence of catalysts. *Chemosphere* 2008;70:453–61.
- Destailhats H, Colussi AJ, Joseph JM, Hoffmann MR. Synergistic effects of sonolysis combined with ozonolysis for the oxidation of azobenzene and methyl orange. *J Phys Chem A* 2000;104:8930–5.
- Ying-Shih M, Chi-Fang S, Jih-Gaw L. Degradation of carbofuran in aqueous solution by ultrasound and Fenton processes: effect of system parameters and kinetic study. *J Hazard Mater* 2010;178:320–5.
- de Luna MG, Veciana ML, Su C, Lu M. Acetaminophen degradation by electro-Fenton and photoelectro-Fenton using a double cathode electrochemical cell. *J Hazard Mater* 2012;217–218:200–7.
- Pollet BG. The use of ultrasound for the fabrication of fuel cell materials. *Int J Hyd. Energy* 2010;35:11986–2004.
- Suslick KS. Applications of ultrasound to materials chemistry. *MRS Bull* 1995 (20):29–34.
- Ashokkumar M, Grieser F. A comparison between multibubble sonoluminescence intensity and the temperature within cavitation bubbles. *J Am Chem Soc* 2005;127:5326–7.
- Ashokkumar M, Lee J, Kentish S, Grieser F. Bubbles in an acoustic field: an overview. *Ultrason Sonochem* 2007;14:470–5.
- Ashokkumar M, Grieser F. Sonochemical preparation of colloids. In: Encyclopedia of surface and colloid science, second ed., New York: Edited by P. Somasundaran, Taylor & Francis; 2006. p. 5685–99.
- Ashokkumar M, Hall R, Mulvaney P, Grieser F. Sonoluminescence from aqueous alcohol and surfactant solutions. *J Phys Chem B* 1997;101:10845–50.
- Ashokkumar M, Grieser F. Single-bubble sonophotoluminescence. *J Am Chem Soc* 2000;122:12001–2.
- Ashokkumar M, Crum LA, Frenley CA, Grieser F, Matula TJ, McNamara III WB, et al. Effect of solutes on single-bubble sonoluminescence in water. *J Phys Chem A* 2000;104:8462–5.
- Rivas DF, Ashokkumar M, Leong T, Yasui K, Tuziuti T, Kentish S, et al. Sonoluminescence and sonochemiluminescence from a microreactor. *Ultrason Sonochem* 2012;19:1252–9.
- Flint EB, Suslick KS. The temperature of cavitation. *Science* 1991;253:1397–9.
- Suslick K. Sonochemistry. *Science* 1990;247:1439–45.
- Suslick KS. The chemical effects of ultrasound. *Sci Am* 1989;80:260–6.
- Margulis M. Sonochemistry and cavitation; OPA (Amsterdam). New York: B. V. Gordon and Breach Science Publ.; 1995.
- Margulis MA. Fundamental aspects of sonochemistry. *Ultrasonics* 1992;30:152–5.

- [53] Lepoint T, Mullie F. What exactly is cavitation chemistry. *Ultrason Sonochem* 1994;1:S13–22.
- [54] Hua I, Hochemer RH, Hoffmann MR. Sonolytic hydrolysis of p-nitrophenyl acetate: the role of supercritical water. *J Phys Chem* 1995;99:2335–42.
- [55] Lida Y, Ashokkumar M, Tuziuti T, Kozuka T, Yasui K, Towata A, et al. Bubble population in sonochemical reactor: I. Estimation of bubble size distribution and its number density with pulsed sonication – laser diffraction method. *Ultrason Sonochem* 2010;17:473–9.
- [56] Lida Y, Ashokkumar M, Tuziuti T, Kozuka T, Yasui K, Towata A, et al. Bubble population in sonochemical reactor: II. Estimation of bubble size distribution and its number density with pulsed sonication – laser diffraction method. *Ultrason Sonochem* 2010;17:480–6.
- [57] Ashokkumar M, Grieser F. *J Am Chem Soc* 2006;127:5326–7.
- [58] Gogate PR. Treatment of wastewater streams containing phenolic compounds using hybrid techniques based on cavitation: a review of the current status and the way forward. *Ultrason Sonochem* 2008;15:1–15.
- [59] Asakura Y, Nishida T, Matsuoka T, Koda S. Effects of ultrasonic frequency and liquid height on sonochemical efficiency of large-scale sonochemical reactors. *Ultrason Sonochem* 2008;15:244–50.
- [60] Okitsu K, Ashokkumar M, Grieser F. Sonochemical synthesis of gold nanoparticles: effects of ultrasound frequency. *J Phys Chem B* 2005;109:20673–5.
- [61] He Y, Vinodgopal K, Ashokkumar M, Grieser F. Sonochemical synthesis of ruthenium nanoparticles. *Res Chem Int* 2006;32:709–15.
- [62] Drijvers D, de Baets R, de Visscher A, Langenhove HV. Sonolysis of trichloroethylene in aqueous solution: volatile organic intermediates. *Ultrason Sonochem* 1996;3:S83–90.
- [63] Madhavan J, Sathishkumar P, Anandan S, Grieser F, Ashokkumar M. Degradation of acid red 88 by the combination of sonolysis and photocatalysis. *Sep Purif Technol* 2010;74:336–41.
- [64] Madhavan J, Grieser F, Ashokkumar M. Degradation of formetanate hydrochloride by combined advanced oxidation processes. *Sep Purif Technol* 2010;73:409–14.
- [65] Madhavan J, Grieser F, Ashokkumar M. Degradation of orange-G by advanced oxidation processes. *Ultrason Sonochem* 2010;17:338–43.
- [66] Madhavan J, Grieser F, Ashokkumar M. Combined advanced oxidation processes for the synergistic degradation of ibuprofen in aqueous environments. *J Hazard Mater* 2010;178:202–8.
- [67] Madhavan J, Sathishkumar P, Anandan S, Grieser F, Ashokkumar M. Sonophotocatalytic degradation of monocrotophos using TiO<sub>2</sub> and Fe<sup>3+</sup>. *J Hazard Mater* 2010;177:944–9.
- [68] Lorimer JP, Mason TJ. Sonochemistry: Part 1 – the physical aspects. *Chem Soc Rev* 1987;16(16):239–74.
- [69] Luche JL. The sonochemistry group organometallic sonochemistry: successes, problems, and byproducts. *Ultrasonics* 1987;25:40–4.
- [70] Anandan S, Ashokkumar M, Grieser F. Sonochemical synthesis of Au–Ag core-shell bimetallic nanoparticles. *J Phys Chem C* 2008;112:15102–5.
- [71] Vinodgopal K, He Y, Ashokkumar M, Grieser F. Sonochemically prepared platinum-ruthenium bimetallic nanoparticles. *J Phys Chem B* 2006;110:3849–52.
- [72] Sathishkumar P, Manivel A, Anandan S, Zhou M, Grieser F, Ashokkumar M. Sonochemical synthesis and characterization of gold–ruthenium bimetallic nanoparticles. *Colloids Surf A: Physicochem Eng Aspects* 2010;356:14–144.
- [73] Kan C, Cai W, Li C, Zhang L, Hofmeister H. Ultrasonic synthesis and optical properties of Au/Pd bimetallic nanoparticles in ethylene glycol. *J Phys D: Appl Phys* 2003;36:1609–14.
- [74] Mazzone G, Rivalta I, Russo N, Sicilia E. Interaction of CO with PdAu(1 1 1) and PdAu(1 0 0) bimetallic surfaces: a theoretical cluster model study. *J Phys Chem C* 2008;112:6073–81.
- [75] Miyamura H, Matsubara R, Kobayashi S. Gold–platinum bimetallic clusters for aerobic oxidation of alcohols under ambient conditions. *Chem Commun* 2008;1:2031–3.
- [76] Toshihima N, Yonezawa T, Harada M, Asakura K, Iwasawa Y. The polymer-protected Pd–Pt bimetallic clusters having catalytic activity for selective hydrogenation of diene. Preparation and EXAFS investigation on the structure. *Chem Lett* 1990;19:815–8.
- [77] Yang J, Lee JY, Too HP. Phase-transfer identification of core-shell structures in bimetallic nanoparticles. *Plasmonics* 2006;1:67–78.
- [78] Shchukin DG, Radziuk D, Mohwald H. Ultrasonic fabrication of metallic nanomaterials and nanoalloys. *Annu Rev Mater Res* 2010;40:345–62.
- [79] Sahoo NG, Rana S, Cho JW, Li L, Chan SH. Polymer nanocomposites based on functionalized carbon nanotubes. *Prog Polym Sci* 2010;35:837–67.
- [80] Rozenberg BA, Tenne R. Polymer-assisted fabrication of nanoparticles and nanocomposites. *Prog Polym Sci* 2008;33:40–112.
- [81] Hussain F, Hojjati M, Okamoto M, Gorga RE. *J Compos Mater* 2006;40:1511–75.
- [82] Ibsi M, Brown B. Variation of the relative intensity of cavitation with temperature. *J Acoust Soc Am* 1967;41:568–72.
- [83] Ley SV. *Low CMR. Ultrasound in synthesis*. Berlin: Springer-Verlag; 1989.
- [84] Moulton KJ, Koritala S, Frankel EN. Ultrasonic hydrogenation of soybean oil. *J Am Oil Chem Soc* 1983;60:1257–8.
- [85] Moulton KJ, Koritala S, Warner K, Frankel EN. Continuous ultrasonic hydrogenation of soybean oil. II. Operating conditions and oil quality. *J Am Oil Chem Soc* 1987;64:542–7.
- [86] Son Y, Lim M, Khim J, Kim L, Ashokkumar M. Comparison of calorimetric energy and cavitation energy for the removal of bisphenol-A: the effects of frequency and liquid height. *Chem Eng J* 2012;183:39–45.
- [87] Bahena CL, Martinez SS, Guzman DM, del M, Hernandez RT. Sonophotocatalytic degradation of alazine and gesaprim commercial herbicides in TiO<sub>2</sub> slurry. *Chemosphere* 2008;71:982–9.
- [88] Kanthale PM, Brochie A, Ashokkumar M, Grieser F. Experimental and theoretical investigations on sonoluminescence under dual frequency conditions. *Ultrason Sonochem* 2008;15:629–35.
- [89] Son Y, Lim M, Khim J, Ashokkumar M. Attenuation of UV light in large-scale sonophotocatalytic reactors: The effects of ultrasound irradiation and TiO<sub>2</sub> concentration. *Ind Eng Chem Res* 2012;51:232–9.
- [90] Ahmedchekkat F, Medjram MS, Chiha M, Ali Al-bsoul AM. Sonophotocatalytic degradation of Rhodamine B using a novel reactor geometry: effect of operating conditions. *Chem Eng J* 2011;178:244–51.
- [91] Kormann C, Bahnemann DW, Hoffmann MR. Photocatalytic production of hydrogen peroxides and organic peroxides in aqueous suspensions of titanium dioxide, zinc oxide, and desert sand. *Environ Sci Technol* 1988;22:798–806.
- [92] Hera N, Parka JS, Yoon Y. Sonochemical enhancement of hydrogen peroxide production by inert glass beads and TiO<sub>2</sub>-coated glass beads in water. *Chem Eng J* 2011;166:184–90.
- [93] Gogate PR, Pandit AB. Sonophotocatalytic reactors for wastewater treatment: a critical Review. *AIChE J* 2004;50:1051–79.
- [94] Sathish Kumar P, Manivel A, Anandan S. Synthesis of Ag–ZnO nanorod for enhanced photocatalytic degradation of Acid Red 88 in aqueous environment. *Water Sci Technol* 2009;59:1423–30.
- [95] Anandan S. Photocatalytic effects of titania supported nanoporous MCM-41 on degradation of methyl orange in the presence of electron acceptors. *Dyes Pigm* 2008;76:535–41.
- [96] Anandan S, Sathish Kumar P, Pugazhenthiran N, Madhavan J, Maruthamuthu P. Effect of loaded silver nanoparticles on TiO<sub>2</sub> for photocatalytic degradation of Acid Red 88. *Sol Energy Mater Sol Cells* 2008;92:929–37.
- [97] Ashokkumar M. The characterization of acoustic cavitation bubbles – an overview. *Ultrason Sonochem* 2011;18:864–72.
- [98] Mishra KP, Gogate PR. Intensification of degradation of aqueous solutions of Rhodamine B using sonochemical reactors at operating capacity of 7 L. *J Environ Manag* 2011;92:1972–7.
- [99] Saharan VK, Pandit AB, Sathish Kumar P, Anandan S. Hydrodynamic cavitation as an advanced oxidation technique for the degradation of Acid Red 88 dye. *Ind Eng Chem Res* 2012;51:1981–9.
- [100] Saharan VK, Badve MP, Pandit AB. Degradation of Reactive Red 120 dye using hydrodynamic cavitation. *Chem Eng J* 2011;178:100–7.
- [101] Ohtani B. Photocatalysis A to Z What we know and what we do not know in a scientific sense. *J Photochem Photobiol C Rev* 2010;11:157–78.
- [102] Horikoshi S, Serpone N. Photochemistry with microwaves catalysts and environmental applications. *J Photochem Photobiol C Rev* 2009;10:96–110.
- [103] Rajeshwar K, Osugi ME, Chanmanee W, Chenthamarakshan CR, Zaroni MVB, Kajitvichyanukul P, et al. Heterogeneous photocatalytic treatment of organic dyes in air and aqueous media. *J Photochem Photobiol C: Photochem Rev* 2008;9:171–92.
- [104] Shiraiishi Y, Hirai T. Selective organic transformations on titanium oxide-based photocatalysts. *J Photochem Photobiol C: Photochem Rev* 2008;9:157–70.
- [105] Demeestere K, Dewulf J, Langenhove HV. Heterogeneous photocatalysis as an advanced oxidation process for the abatement of chlorinated, monocyclic aromatic and sulfurous volatile organic compounds in air: state of the art. *Crit Rev Environ Sci Technol* 2007;37:489–538.
- [106] Chen X, Mao SS. Titanium dioxide nanomaterials: synthesis, properties, modifications, and applications. *Chem Rev* 2007;107:2891–959.
- [107] Anandan S, Yoon M. Photocatalytic activities of the nano-sized TiO<sub>2</sub>-supported Y-zeolites. *J Photochem Photobiol C Photochem Rev* 2003;4:5–18.
- [108] Chatterjee D, Dasgupta S. Visible light induced photocatalytic degradation of organic pollutants. *J Photochem Photobiol C: Photochem Rev* 2005;6:186–205.
- [109] Hoffmann MR, Martin ST, Choi W, Bahnemann DW. Environmental applications of semiconductor photocatalysis. *Chem Rev* 1995;95:69–96.
- [110] Fox MA, Dulay MT. Heterogeneous photocatalysis. *Chem Rev* 1993;93:341–57.
- [111] Kalyansundaram K, Gratzel M. Interfacial electron transfer in colloidal metal and semiconductor dispersions and photodecomposition of water. *Coord Chem Rev* 1986;69:57–125.
- [112] Nozik AJ. Photoelectrochemistry: applications to solar energy conversion. *Ann Rev Phys Chem* 1978;29:189–222.
- [113] Kamat PV. Photochemistry on nonreactive and reactive (semiconductor) surfaces. *Chem Rev* 1993;93:267–300.
- [114] Mills A, Davies RH, Worsley D. *Chem Soc Rev* 1993;22:417–25.
- [115] Mills A, Davis RH, Worsley D. Water purification by semiconductor photocatalysis. *Chem Soc Rev* 1993;22:417–25.
- [116] Kuhnlein HV, Chan HM. Environment and contaminants in traditional food systems of northern indigenous peoples. *Annu Rev Nutr* 2000;20:595–626.
- [117] Kamat PV, Meisel D. Nanoparticles in advanced oxidation processes. *Curr Opin Colloid Interface Sci* 2002;7:282–7.
- [118] Konstantinou IK, Albanis TA. TiO<sub>2</sub>-assisted photocatalytic degradation of azo dyes in aqueous solution: kinetic and mechanistic investigations: a review. *Appl Catal B Environ* 2004;49:1–14.
- [119] Kabra K, Chaudhary R, Sawhney RL. Treatment of hazardous organic and inorganic compounds through aqueous-phase photocatalysis: a review. *Ind Eng Chem Res* 2004;43:7683–96.

- [120] Abrams BL, Wilcoxon JP. Nanosize semiconductors for photooxidation. *Crit Rev Solid State Mater Sci* 2005;30:153–82.
- [121] Chatterjee D. Effect of excited state redox properties of dye sensitizers on hydrogen production through photosplitting of water over TiO<sub>2</sub> photocatalyst. *Catal Commun* 2010;11:336–9.
- [122] Dhananjeyan MR, Fine E, Kiwi J. Synthetic polymer delivery system: sustained release of persulfate during the photo-oxidation of an azo-dye. *J Photochem Photobiol A: Chem* 2000;136:125–31.
- [123] Suppan P. *Chemistry and light*. Cambridge: Royal Society of Chemistry; 1994. p. 5.
- [124] Porter G. *Light, chemical change and life: a source book in photochemistry*. In: Coyle JD, Hill RR, Roberts DR, editors. Milton Keynes: Open University Press; 1982. p. 355.
- [125] Pichat P, Mozzanega MN, Coufoou H. Investigation of the mechanism of photocatalytic alcohol dehydrogenation over Pt/TiO<sub>2</sub> using poisons and labelled ethanol. *J Chem Soc Faraday Trans* 1987;83:697–704.
- [126] Borgarello E, Harris R, Serpone N. Photochemical deposition and photo-recovery of gold using semiconductor dispersions. Practical application of photocatalysis. *Nouv J Chim* 1985;9:743–7.
- [127] Han Z, Chang V, Wang X, Lim T, Hildemann L. Experimental study on visible-light induced photocatalytic oxidation of gaseous formaldehyde by polyester fiber supported photocatalysts. *Chem Eng J* 2013;218:9–18.
- [128] Lewis NS, Nocera DG. Powering the planet: chemical challenges in solar energy utilization. *Proc Natl Acad Sci USA* 2006;103:15729–35.
- [129] Lewis NS, Crabtree G, Nozik AJ, Wasielewski MR, Alivisatos AP. Basic research needs for solar energy utilization. Washington, DC: U.S. Department of Energy; 2005.
- [130] Abe R. Recent progress on photocatalytic and photoelectrochemical water splitting under visible light irradiation. *J Photochem Photobiol C Rev* 2010;11:179–209.
- [131] Ni M, Leung MKH, Leung DYC, Sumathy K. A review and recent developments in photocatalytic water-splitting using TiO<sub>2</sub> for hydrogen production. *Renew Sustain Energy Rev* 2007;11:401–25.
- [132] Raissi AT, Muradov N, Huang C, Adebisi O. Hydrogen from solar via light-assisted high-temperature water splitting cycles. *J Sol Energy Eng* 2007;129:184–9.
- [133] Sathishkumar P, Pugazhenthiran N, Mangalaraja RV, Asiri AM, Anandan S. ZnO supported CoFe<sub>2</sub>O<sub>4</sub> nanophotocatalysts for the mineralization of Direct Blue 71 in aqueous environments. *J Hazard Mater* 2013;252–253:171–9.
- [134] Sathishkumar P, Mangalaraja RV, Anandan S, Ashokkumar M. CoFe<sub>2</sub>O<sub>4</sub>/TiO<sub>2</sub> nanocatalysts for the photocatalytic degradation of Reactive Red 120 in aqueous solutions in the presence and absence of electron acceptors. *Chem Eng J* 2013;220:302–10.
- [135] Sathishkumar P, Mangalaraja RV, Anandan S, Ashokkumar M. Photocatalytic degradation of ternary dyestuff mixture in aqueous environment using gold nanoparticles loaded amino and mercapto functionalized TiMCM-41 nanocatalysts in the presence of visible light. *Sep Purif Technol* 2013;102:67–74.
- [136] Pugazhenthiran N, Sathishkumar P, Maruthamuthu P, Anandan S. HPA immobilized on the functionalized TiMCM-41 nanochannels for photocatalytic degradation of ternary dyestuff effluent. *J Porous Mater* 2013;20:489–99.
- [137] Anandan S, Lee G, Yang C, Ashokkumar M, Wu JJ. Sonochemical synthesis of Bi<sub>2</sub>CuO<sub>4</sub> nanoparticles for catalytic degradation of nonylphenol ethoxylate. *Chem Eng J* 2012;183:46–52.
- [138] Anandan S, Lee G, Hsieh S, Ashokkumar M, Wu JJ. Amorphous titania-coated magnetite spherical nanoparticles: sonochemical synthesis and catalytic degradation of nonylphenol ethoxylate. *Ind Eng Chem Res* 2011;50:7874–81.
- [139] Sathish Kumar P, Anandan S, Maruthamuthu P, Swaminathan T, Ashokkumar M. Synthesis of visible light activated crystalline Fe<sup>3+</sup> doped TiO<sub>2</sub> nanophotocatalysts for the degradation of azo dye. *Colloid Surf A: Phys Eng Aspects* 2011;375:231–6.
- [140] Sathish Kumar P, Sweena R, Wu JJ, Anandan S. Synthesis of CuO–ZnO nanophotocatalyst for visible light assisted degradation of a textile dye in aqueous solution. *Chem Eng J* 2011;171:136–40.
- [141] Pugazhenthiran N, Sathish Kumar P, Murugesan S, Anandan S. Effective degradation of acid orange 10 by catalytic ozonation in presence of Au–Bi<sub>2</sub>O<sub>3</sub> nanoparticles. *Chem Eng J* 2011;168:1227–33.
- [142] Sathish Kumar P, Ruby Raj M, Anandan S. Nanoporous Au–TiMCM-41 – an inorganic hybrid photocatalyst toward visible photooxidation of methyl orange. *Sol Energy Mater Sol Cells* 2010;94:1783–9.
- [143] Pugazhenthiran N, Ramkumar S, Sathish Kumar P, Anandan S. In-situ preparation of heteropolytungstic acid on TiMCM-41 nanoporous framework for photocatalytic degradation of textile dye methyl orange. *Micropor Mesopor Mater* 2010;131:170–6.
- [144] Sathish Kumar P, Ruby Raj M, Anandan S, Zhou M, Ashokkumar M. Study of Au–ZnO nanophotocatalysts toward visible photodegradation of Acid Red 88 in aqueous solutions. *Water Sci Technol* 2009;60:1589–96.
- [145] Sathishkumar P, Mangalaraja RV, Rozas O, Vergara C, Mansilla HD, Gracia-Pinilla MA, et al. Sonophotocatalytic mineralization of Norflurazon in aqueous environment. *Chemosphere* 2015(xx): xxx–xxx.
- [146] Anandan S, Yoon M. Photocatalytic degradation of methyl orange using heteropolytungstic acid-encapsulated TiSBA-15. *Solar Energy Mater. Solar Cells* 2007;91:143–7.
- [147] Sathish Kumar P, Sivakumar R, Anandan S, Madhavan J, Maruthamuthu P, Ashokkumar M. Study of Au–TiO<sub>2</sub> photocatalysts toward visible photodegradation of acid red 88 in the presence of electron acceptors. *Water Res* 2008;42:4878–84.
- [148] Sathishkumar P, Mangalaraja RV, Mansilla HD, Gracia-Pinilla MA, Anandan S. Sonophotocatalytic (42 kHz) degradation of Simazine in the presence of Au–TiO<sub>2</sub> nanocatalysts. *Appl Catal B: Environ* 2014;160–161:692–700.
- [149] Anandan S, Yoon M, Park SE. Photocatalytic effects of heteropolytungstic acid-encapsulated TiSBA-15 on decomposition of phenol. *J Photosci* 2003;10:231–6.
- [150] Anandan S, Ryu SY, Cho WJ, Yoon M. Heteropolytungstic acid (H<sub>3</sub>PW<sub>12</sub>O<sub>40</sub>)-encapsulated into the titanium-exchanged HY(TiHY) zeolite: a novel photocatalyst for photoreduction of methyl orange. *J Mol Catal A: Chem* 2003;195:201–8.
- [151] Miranda C, Mansilla H, Yanez J, Obregon S, Colon G. Improved photocatalytic activity of g-C<sub>3</sub>N<sub>4</sub>/TiO<sub>2</sub> composites prepared by a simple impregnation method. *J Photochem Photobiol A: Chem* 2013;253:16–21.
- [152] Muruganandham M, Amutha R, Wahed MSMA, Ahmmad B, Kuroda Y, Suri RPS, et al. Controlled fabrication of α-GaOOH and α-Ga<sub>2</sub>O<sub>3</sub> self-assembly and its superior photocatalytic activity. *J Phys Chem C* 2012;116:44–53.
- [153] Huang J, Wang X, Hou Y, Chen X, Wu L, Fu X. Degradation of benzene over a zinc germanate photocatalyst under ambient conditions. *Environ Sci Technol* 2008;42:7387–91.
- [154] Sun M, Li D, Zhang W, Fu X, Shao Y, Li W, et al. Rapid microwave hydrothermal synthesis of GaOOH nanorods with photocatalytic activity toward aromatic compounds. *Nanotechnology* 2010;21(7pp):355601.
- [155] Anandan S, Pugazhenthiran N, Selvamani T, Hsieh S, Lee G, Wu JJ. Investigation on photocatalytic potential of Au-Ta<sub>2</sub>O<sub>5</sub> semiconductor nanoparticle by degrading Methyl Orange in aqueous solution by illuminating with visible light. *Catal Sci Technol*. 2012;2:2502–7.
- [156] Cao J, Li X, Lin H, Xu B, Chen S, Guan Q. Surface acid etching of (BiO)<sub>2</sub>CO<sub>3</sub> to construct (BiO)<sub>2</sub>CO<sub>3</sub>/BiOX (X=Cl, Br, I) heterostructure for methyl orange removal under visible light. *Appl Surf Sci* 2013;266:294–9.
- [157] Yang SJ, Im JH, Kim T, Lee K, Park CR. MOF-derived ZnO and ZnO@C composites with high photocatalytic activity and adsorption capacity. *J Hazard Mater* 2011;186:376–82.
- [158] Hengky C, Moya X, Mathur ND, Dunn S. Evidence of high rate visible light photochemical decolourisation of Rhodamine B with BiFeO<sub>3</sub> nanoparticles associated with BiFeO<sub>3</sub> photocorrosion. *RSC Adv* 2012;2:11843–9.
- [159] Hengky C, Dunn S. Photocatalytic decolourisation of RhB and photocorrosion of BiFeO<sub>3</sub>. *MRS Proc* 2012. <http://dx.doi.org/10.1557/opl.2012.1190> mrs12-1443-r01-12.
- [160] Neppolian B, Choi HC, Sakthivel S, Arabindoo B, Murugesan V. Solar/UV-induced photocatalytic degradation of three commercial textile dyes. *J Hazard Mater B* 2002;89:303–17.
- [161] Ziyilan-Yavas A, Mizukoshi Y, Maeda Y, Ince NH. Supporting of pristine TiO<sub>2</sub> with noble metals to enhance the oxidation and mineralization of paracetamol by sonolysis and sonophotolysis. *Appl Catal B: Environ* 2015;172–173:7–17.
- [162] Soleymani AR, Saïen J, Chin S, Le HA, Park E, Jurng J. Modeling and optimization of a sono-assisted photocatalytic water treatment process via central composite design methodology. *Process Saf Environ* 2015;94:307–14.
- [163] Im J, Yoon J, Her N, Han J, Zoh K, Yoon Y. Sonocatalytic-TiO<sub>2</sub> nanotube, Fenton, and CCl<sub>4</sub> reactions for enhanced oxidation, and their applications to acetaminophen and naproxen degradation. *Sep Purif Technol* 2015;141:1–9.
- [164] Ziyilan A, Ince NH. Catalytic ozonation of ibuprofen with ultrasound and Fe-based catalysts. *Catal Today* 2015;240:2–8.
- [165] Drosou C, Coz A, Xekoukoulotakis NP, Moya A, Vergara Y, Mantzavinos D. Peracetic acid-enhanced photocatalytic and sonophotocatalytic inactivation of *E. coli* in aqueous suspensions. *J Chemtech Biotech* 2010;85:1049–53.
- [166] An T, Gu H, Xiong Y, Chen W, Zhu X, Sheng G, et al. Decolourization and COD removal from reactive dye-containing wastewater using sonophotocatalytic technology. *Chemtech Biotech* 2003;78:1142–8.
- [167] Hemapriyamvadha R, Sivasankar T. Sonophotocatalytic treatment of methyl orange dye and real textile effluent using synthesised nano-zinc oxide. *Color Technol* 2015;131:110–9.
- [168] Eren Z. Degradation of an azo dye with homogeneous and heterogeneous catalysts by sonophotolysis. *Clean – Soil, Air, Water* 2012;40:1284–9.
- [169] Arai T, Yanagida M, Konishi Y, Iwasaki Y, Sugihara H, Sayama K. Efficient complete oxidation of acetaldehyde into CO<sub>2</sub> over CuBi<sub>2</sub>O<sub>4</sub>/WO<sub>3</sub> composite photocatalyst under visible and UV light irradiation. *J Phys Chem C* 2007;111:7574–7.
- [170] Liu W, Chen S, Zhang S, Zhao W, Zhang H, Yu XJ. Preparation and characterization of p-n heterojunction photocatalyst p-CuBi<sub>2</sub>O<sub>4</sub>/n-TiO<sub>2</sub> with high photocatalytic activity under visible and UV light irradiation. *J Nanopart Res* 2010;12:1355–66.
- [171] Manivel A, Naveenraj S, Sathish Kumar P, Anandan S. CuO–TiO<sub>2</sub> nanocatalyst for UV-photodegradation of Acid Red 88 in aqueous solution. *Sci Adv Mater* 2010;2:51–7.
- [172] Kubo M, Fukuda H, Chua XJ, Yonemoto T. Kinetics of ultrasonic degradation of phenol in the presence of composite particles of titanium dioxide and activated carbon. *Ind Eng Chem Res* 2007;46:699–704.
- [173] Meng Z, Zhu L, Choi J, Park CY, Oh W. Sonocatalytic degradation of Rhodamine B in the presence of C60 and CdS coupled TiO<sub>2</sub> particles. *Ultrason Sonochem* 2012;19:143–50.
- [174] Joseph CG, Puma GL, Bono A, Taufiq-Yap YH, Krishnaiah D. Operating parameters and synergistic effects of combining ultrasound and ultraviolet

- irradiation in the degradation of 2,4,6-trichlorophenol. *Desalination* 2011;276:303–9.
- [175] He Y, Grieser F, Ashokkumar M. The mechanism of sonophotocatalytic degradation of methyl orange and its products in aqueous solutions. *Ultrason Sonochem* 2011;18:974–80.
- [176] Wang N, Zhu L, Wang M, Wang D, Tang H. Sono-enhanced degradation of dye pollutants with the use of  $\text{H}_2\text{O}_2$  activated by  $\text{Fe}_3\text{O}_4$  magnetic nanoparticles as peroxidase mimetic. *Ultrason Sonochem* 2010;17:78–83.
- [177] Kaur S, Singh V. Visible light induced sonophotocatalytic degradation of Reactive Red dye 198 using dye sensitized  $\text{TiO}_2$ . *Ultrason Sonochem* 2007;14:531–7.
- [178] Zhang K, Oh W. Kinetic study of the visible light-induced sonophotocatalytic degradation of MB solution in the presence of  $\text{Fe}/\text{TiO}_2$ -MWCNT catalyst. *Bull Korean Chem Soc* 2010;31:1589–95.
- [179] Neppolian B, Ciceri L, Bianchi CL, Grieser F, Ashokkumar M. Sonophotocatalytic degradation of 4-chlorophenol using  $\text{Bi}_2\text{O}_3/\text{TiZrO}_4$  as a visible light responsive photocatalyst. *Ultrason Sonochem* 2011;18:135–9.
- [180] Sajen J, Delavari H, Solymani AR. Sono-assisted photocatalytic degradation of styrene-acrylic acid copolymer in aqueous media with nano titania particles and kinetic studies. *J Hazard Mater* 2010;177:1031–8.
- [181] Mrowetz M, Pirola C, Selli E. Degradation of organic water pollutants through sonophotocatalysis in the presence of  $\text{TiO}_2$ . *Ultrason Sonochem* 2003;10:247–54.
- [182] Chen W, Huang S. Sonophotocatalytic degradation of dinitrotoluenes and trinitrotoluene in industrial wastewater. *Chem Eng J* 2011;172:944–51.
- [183] Safavi A, Momeni S. Highly efficient degradation of azo dyes by palladium/hydroxyapatite/ $\text{Fe}_3\text{O}_4$  nanocatalyst. *J Hazard Mater* 2012;201–202:125–31.
- [184] Chen Y, Vorontsov AV, Smirniotis PG. Enhanced photocatalytic degradation of dimethyl methylphosphonate in the presence of low-frequency ultrasound. *Photochem Photobiol Sci* 2003;2:694–8.
- [185] Hapeshi E, Fotiou I, Fatta-Kassinos D. Sonophotocatalytic treatment of ofloxacin in secondary treated effluent and elucidation of its transformation products. *Chem Eng J* 2013;224:96–105.
- [186] Stavarache C, Yim B, Vinatoru M, Maeda Y. Sonolysis of chlorobenzene in Fenton-type aqueous systems. *Ultrason Sonochem* 2002;9:291–6.
- [187] Yasman Y, Bulatov V, Gridin VV, Agur S, Galil N, Armon R, et al. A new sono-electrochemical method for enhanced detoxification of hydrophilic chloro-organic pollutants in water. *Ultrason Sonochem* 2004;11:365–72.
- [188] Klavarioti M, Mantzavinos D, Kassinos D. Removal of residual pharmaceuticals from aqueous systems by advanced oxidation processes. *Environ Int* 2009;35:402–17.
- [189] Balu AM, Baruwati B, Serrano E, Cot J, Garcia-Martinez J, Varma RS, et al. Magnetically separable nanocomposites with photocatalytic activity under visible light for the selective transformation of biomass-derived platform molecules. *Green Chem* 2011;13:2750–8.
- [190] Herrmann JM, Tahir H, Guillard C, Pichat P. Photocatalytic degradation of aqueous hydroxy-butandioic acid (malic acid) in contact with powdered and supported titania in water. *Catal Today* 1999;54:131.
- [191] Riaz U, Ashraf SM. Latent photocatalytic behavior of semi-conducting poly (1-naphthylamine) nanotubes in the degradation of Comassie Brilliant Blue RG-250. *Sep Purif Technol* 2012;95:97–102.
- [192] Panchangam SC, Lin AY, Tsai JH, Lin CF. Sonication-assisted photocatalytic decomposition of perfluorooctanoic acid. *Chemosphere* 2009;75:654–60.
- [193] Khokhawala IM, Gogate PR. Degradation of phenol using a combination of ultrasonic and UV irradiations at pilot scale operation. *Ultrason Sonochem* 2010;17:833–8.
- [194] Chen Y, Smirniotis P. Enhancement of photocatalytic degradation of phenol and chlorophenols by ultrasound. *Ind Eng Chem Res* 2002;41:5958–65.
- [195] An T, Gu H, Xiong Y, Chen W, Zhu X, Sheng G, et al. Decolorization and COD removal from reactive dye-containing wastewater using sonophotocatalytic technology. *J Chem Technol Biotechnol* 2003;78:142–148.
- [196] Cui P, Chen Y, Chen G. Degradation of low concentration methyl orange in aqueous solution through sonophotocatalysis with simultaneous recovery of photocatalyst by ceramic membrane microfiltration. *Ind Eng Chem Res* 2011;50:3947–54.
- [197] Selli E. Synergistic effects of sonolysis combined with photocatalysis in the degradation of an azo dye. *Phys Chem Chem Phys* 2002;4:6123–8.
- [198] Vajnhandl S, Marechal AML. Ultrasound in textile dyeing and the decoloration/mineralization of textile dyes. *Dyes Pigm* 2005;65:89–101.
- [199] Gultekin I, Ince NH. Synthetic endocrine disruptors in the environment and water remediation by advanced oxidation processes. *J Environ Manag* 2007;85:816–32.
- [200] Tokumoto T, Ishikawa K, Furusawa T, Ii S, Hachisuka K, Tokumoto M, et al. Sonophotocatalysis of endocrine-disrupting chemicals. *Mar Environ. Res.* 2008;66:372–7.
- [201] Silva AMT, Nouli E, Carmo-Apolinario AC, Xekoukoulotakis NP, Mantzavinos D. Sonophotocatalytic/ $\text{H}_2\text{O}_2$  degradation of phenolic compounds in agro-industrial effluents. *Catal Today* 2007;124:232–9.
- [202] Zouaghi R, David B, Suptil J, Djebbar K, Boutiti A, Guittonneau S. Sonochemical and sonocatalytic degradation of monolinuron in water. *Ultrason Sonochem* 2011;18:1107–12.
- [203] Abu-Hassan MA, Kim JK, Metcalfe IS, Mantzavinos D. Kinetics of low frequency sonodegradation of linear alkylbenzene sulfonate solutions. *Chemosphere* 2006;62:749–55.
- [204] Nakajima A, Tanaka M, Kameshima Y, Okada K. Sonophotocatalytic destruction of 1,4-dioxane in aqueous systems by HF-treated  $\text{TiO}_2$  powder. *J Photochem Photobiol A: Chem* 2004;167:75–9.
- [205] Selli E, Bianchi CL, Pirola C, Cappelletti G, Ragaini V. Efficiency of 1,4-dichlorobenzene degradation in water under photolysis, photocatalysis on  $\text{TiO}_2$  and sonolysis. *J Hazard Mater* 2008;153:1136–41.
- [206] Anandan S, Ashokkumar M. Sonochemical synthesis of Au- $\text{TiO}_2$  nanoparticles for the sonophotocatalytic degradation of organic pollutants in aqueous environment. *Ultrason Sonochem* 2009;16:316–20.
- [207] He Y, Grieser F, Ashokkumar M. Kinetics and mechanism for the sonophotocatalytic degradation of p-chlorobenzoic acid. *J Phys Chem A* 2011;115:6582–8.
- [208] Singla R, Grieser F, Ashokkumar M. The mechanism of sonochemical degradation of a cationic surfactant in aqueous solution. *Ultrason Sonochem* 2011;18:484–8.
- [209] Singla R, Grieser F, Ashokkumar M. Sonochemical degradation of Martius Yellow dye in aqueous solution. *Ultrason Sonochem* 2009;16:28–34.
- [210] Mohammadi M, Sabbaghi S. Photo-catalytic degradation of 2,4-DCP wastewater using MWCNT/ $\text{TiO}_2$  nano-composite activated by UV and solar light. *Environ. Nanotech. Monitor. Manag.* 2014;1–2:24–9.
- [211] Martín de Vidales MJ, Barba S, Sáez C, Cañizares P, Rodrigo MA. Coupling ultraviolet light and ultrasound irradiation with Conductive-Diamond Electrochemical Oxidation for the removal of progesterone. *Electrochim Acta* 2014;140:20–6.
- [212] Jyothi KP, Yesodharan S, Yesodharan EP. Ultrasound (US), ultraviolet light (UV) and combination (US+UV) assisted semiconductor catalysed degradation of organic pollutants in water: oscillation in the concentration of hydrogen peroxide formed in situ. *Ultrason Sonochem* 2014;21:1787–96.
- [213] Wang C, Liu C. Decontamination of alachlor herbicide wastewater by a continuous dosing mode ultrasound/ $\text{Fe}^{2+}/\text{H}_2\text{O}_2$  process. *J Environ Sci* 2014;26:1332–9.
- [214] Pignatello J, Oliveros E, MacKay A. Advanced oxidation processes for organic contaminant destruction based on the Fenton reaction and related chemistry. *Crit Rev Environ Sci Technol* 2006;36:1–84.
- [215] Brillas E, Sires I, Oturan MA. Electro-Fenton process and related electrochemical technologies based on Fenton's reaction chemistry. *Chem Rev* 2009;109:6570–631.
- [216] Mason TJ, Petrier C. Ultrasound processes. In: Parson S, editor. *Advanced oxidation processes for water and wastewater treatment*. London: IWA Publishing; 2004. p. 185–208.
- [217] Petrier C, Casadonte D. In: Mason TJ, Tiehm A, editors. *Advances in sonochemistry: ultrasound in environmental protection*, 6. Stamford: JAI Press Inc.; 2001. p. 91–109.
- [218] Amorim CC, Leao MMD, Moreira RFFM, Fabris JD, Henriques AB. Performance of blast furnace waste for azo dye degradation through photo-Fenton-like processes. *Chem Eng J* 2013;224:59–66.
- [219] Torres-Palma RA, Nieto JL, Combet E, Petrier C, Pulgarin An C. Innovative ultrasound,  $\text{Fe}^{2+}$  and  $\text{TiO}_2$  photoassisted process for bisphenol A mineralization. *Water research* 2010;44:2245–52.
- [220] Ioan I, Wilson S, Lundanes E, Neculai A. Comparison of Fenton and sono-Fenton bisphenol A degradation. *J Hazard Mater* 2007;142:559–63.
- [221] Chen F, Li Y, Cai W, Zhang J. Preparation and sono-Fenton performance of 4A-zeolite supported  $\alpha\text{-Fe}_2\text{O}_3$ . *J Hazard Mater* 2010;177:743–9.
- [222] Ozcan A, Sahin Y, Koparal AS, Oturan MA. Degradation of picloram by the electro-Fenton process. *J Hazard Mater* 2008;153:718–27.
- [223] Ghauch A. Degradation of benomyl, picloram, and dicamba in a conical apparatus by zero-valent iron powder. *Chemosphere* 2001;43:1109–17.
- [224] Rahman MA, Muneer M. Heterogeneous photocatalytic degradation of picloram, dicamba, and floumeturon in aqueous suspensions of titanium dioxide. *J Environ Sci Health* 2005;40:247–67.
- [225] Pavlovica I, Barrigaa C, Hermosinb MC, Cornejob J, Ulbarri MA. Adsorption of acidic pesticides 2,4-D, clopyralid and picloram on calcined hydrotalcite. *Appl Clay Sci* 2005;30:125–33.
- [226] Chu YY, Qian Y, Wang WJ, Deng XL. A dual-cathode electro-Fenton oxidation coupled with anodic oxidation system used for 4-nitrophenol degradation. *J Hazard Mater* 2012;199–200:179–85.
- [227] Martínez SS, Uribe EV. Enhanced sonochemical degradation of azure B dye by the electroFenton process. *Ultrason Sonochem* 2012;10:174–8.
- [228] Zhong X, Royer S, Zhang H, Huang Q, Xiang L, Valange S, et al. Mesoporous silica iron-doped as stable and efficient heterogeneous catalyst for the degradation of Cl. Acid Orange 7 using sono-photo-Fenton process. *Sep Purif Technol* 2011;80:163–71.
- [229] Cong Y, Li Z, Zhang Y, Wang Q, Xu Q. Synthesis of  $\alpha\text{-Fe}_2\text{O}_3/\text{TiO}_2$  nanotube arrays for photoelectro-Fenton degradation of phenol. *Chem Eng J* 2012;191:356–63.
- [230] Thokchom B, Pandit AB, Qiu P, Park B, Choi J, Khim J. A review on sono-electrochemical technology as an upcoming alternative for pollutant degradation. *Ultrason Sonochem* 2015;27:210–34.
- [231] Lesko T, Colussi AJ, Hoffmann MR. Sonochemical decomposition of phenol: Evidence for a synergistic effect of ozone and ultrasound for the elimination of total organic carbon from water. *Environ Sci Technol* 2006;40:6818–23.
- [232] Wang J, Wang X, Li G, Guo P, Luo Z. Degradation of EDTA in aqueous solution by using ozonolysis and ozonolysis combined with sonolysis. *J Hazard Mater* 2010;176:333–8.

- [233] Weavers LK, Ling FH, Hoffmann MR. Aromatic compound degradation in water using a combination of sonolysis and ozonolysis. *Environ Sci Technol* 1998;32:2727–33.
- [234] Olson T, Barbier P. Oxidation kinetics of natural organic matter by sonolysis and ozone. *Water Res.* 1994;28:1383–91.
- [235] Barbier P, Petrier C. Study at 20 kHz and 500 kHz of the ultrasound-ozone advanced oxidation system: 4-nitrophenol degradation. *J Adv Oxid Technol* 1996;1:154–9.
- [236] Kang J, Hoffmann M. Kinetics and mechanism of the sonolytic destruction of methyl tert-butyl ether by ultrasonic irradiation in the presence of ozone. *Environ Sci Technol* 1998;32:3194–9.
- [237] Muthukumar M, Selvakumar N. Studies on the effect of inorganic salts on decolouration of acid dye effluents by ozonation. *Dyes Pigm* 2004;62:221–8.
- [238] Gogate PR, Pandit AB. A review of imperative technologies for wastewater treatment II: hybrid methods. *Adv Environ Res* 2004;8:553–97.
- [239] Song S, Ying H, He Z, Chen J. Mechanism of decolorization and degradation of CI Direct Red 23 by ozonation combined with sonolysis. *Chemosphere* 2007;66:1782–8.
- [240] Yang L, Hu C, Nie Y, Qu J. Catalytic ozonation of selected pharmaceuticals over mesoporous alumina-supported manganese oxide. *Environ Sci Technol* 2009;43:2525–9.
- [241] Somensi CA, Simionatto EL, Dalmarco JB, Gaspareto P, Radetski CM. A comparison between ozonolysis and sonolysis/ozonolysis treatments for the degradation of the cytostatic drugs methotrexate and doxorubicin: kinetic and efficiency approaches. *J Environ Sci Health Part A* 2012;47:1543–50.
- [242] Agustina TE, Ang HM, Vareek VK. A review of synergistic effect of photocatalysis and ozonation on wastewater treatment. *J Photochem Photobiol C Rev* 2005;6:264–73.